View metadata, citation and similar papers at core.ac.uk
brought to you by CORE
provided by CERN Document Server

August 22, 2001

Phase transition in two-flavor dense QCD from the Schwinger-Dyson equation

Masayasu Harada and Satoshi Takagi

Department of Physics, Nagoya University, Nagoya, 464-8602, Japan

Abstract

We investigate the phase structure of the two-flavor dense QCD using the Schwinger-Dyson equation (SDE) with the improved ladder approximation in the Landau gauge. The SDE for diquark condensate (color superconducting condensate) and that for quark-antiquark condensate (chiral condensate) are solved separately. In the low density region both the SDE's have nontrivial solutions which correspond to the color symmetry breaking (CSB) vacuum and the chiral symmetry breaking (χSB) vacuum. Comparing the values of the effective potential at two vacua, we show that the χSB vacuum is more stable than the CSB vacuum in the low density region, and that the phase transition from the χSB vacuum to the CSB vacuum is of first order. The critical value of the chemical potential at the phase transition point is found to be smaller than that obtained by the SDE-analysis with including only the chiral condensate.

1 Introduction

Dynamical chiral symmetry breaking is one of the most remarkable features in QCD. The QCD Lagrangian of the light quark sector has an approximate chiral symmetry, and it is spontaneously broken by the strong interaction of QCD. Several physical processes of light hadrons in the low-energy region are governed by the chiral symmetry property. In hot and/or dense matter, on the other hand, the chiral condensate (quark-antiquark condensate) melts and the chiral symmetry is restored (for recent reviews, see, e.g., Ref. [1]).

In early days, it was pointed [2, 3] that there exists diquark condensate (color superconducting condensate) in the high density region. Recently, it was shown [4] by using the instanton induced four-Fermi interaction model that the diquark condensate is on the order of 100 MeV. The diquark condensate is not a color singlet, and thus breaks the color gauge symmetry. This phenomenon is called color superconductivity (See, for recent reviews, e.g., Refs. [5].).

There are many works on the color superconductivity by the analysis based on the Schwinger-Dyson equation (SDE) (see, e.g., Refs.[6, 7, 8, 9]). Since the SDE analysis is justified by the weak coupling, most of the works concentrate on the high density region. However, the density inside the neutron star seems close to the phase transition point (see, e.g., Ref. [5]), where the competition between the chiral condensate and the diquark condensate becomes important.

Competition between the chiral condensate and the diquark condensate was studied by several approaches (see, e.g., Refs. [10, 11, 9]). In Ref. [9] the SDE is converted into the algebraic equation using the confining model gluon propagator, and it was shown that the color symmetry breaking vacuum exists as a solution of the SDE even in the low density region but it is less stable than the chiral symmetry breaking vacuum. It is interesting to study whether such a false vacuum exist by fully solving the SDE.

In this paper, we study the phase transition in QCD in dense matter using the SDE with the improved ladder approximation in the Landau gauge. In dense medium, although the electric gluons have Debye masses, the magnetic gluons are not screened. The unscreened magnetic gluons give dominant contribution to the formation of the Majorana mass gap [12, 6, 7]. Then, we include the effects of the Debye screening in the gluon

propagator using the hard dense loop approximation. We solve the SDE's for the Dirac mass and the Majorana mass separately, and determine the true vacuum by comparing the value of the effective potential at the solution.

The symmetry breaking pattern in the color superconducting phase depends on the number of light quarks. When the number of massless quarks is two ($N_f = 2$), the dominant diquark condensate is the singlet of $\mathrm{SU(2)_L \times SU(2)_R}$, and thus the chiral symmetry is not broken, while the color $\mathrm{SU(3)_c}$ is broken down to its subgroup $\mathrm{SU(2)_c}$ (2SC phase) [4]. For three massless quarks ($N_f = 3$), on the other hand, the dominant diquark condensate breaks the color $\mathrm{SU(3)_c}$ and the chiral $\mathrm{SU(3)_L \times SU(3)_R}$ symmetry together into their diagonal subgroup $\mathrm{SU(3)_{c+L+R}}$ (color flavor locking phase: CFL phase) [13]. The breaking pattern in the real QCD depends on the strange quark mass (see, e.g., Ref. [14]). The above two breaking patterns are understood as two limits of the strange quark mass: When the strange quark is heavy enough, the 2SC phase is realized. For the massless strange quark, on the other hand, the CFL phase is realized.

In the present analysis we consider that the strange quark mass is large enough to neglect the strange quark in the formation of the diquark condensate of u and d quarks: We assume that the color superconductivity is realized in 2SC phase. Thus, the Lagrangian we consider in the present analysis is invariant under the chiral $\mathrm{SU(2)_L \times SU(2)_R}$ symmetry. In the low density region this chiral symmetry is broken down to its diagonal subgroup but the color symmetry is unbroken:

$$\mathrm{SU(3)_c \times SU(2)_L \times SU(2)_R \to SU(3)_c \times SU(2)_V} \ .$$

In the high density region, on the other hand, the chiral symmetry is restored but the color symmetry is broken down to its subgroup [4]:

$$\mathrm{SU(3)_c \times SU(2)_L \times SU(2)_R \to SU(2)_c \times SU(2)_L \times SU(2)_R} \ .$$

This paper is organized as follows. In Sec. 2, we summarize the quark propagator, the gluon propagator and the running coupling which we use in the present analysis. Several approximations to the quark propagator are made. We also give formulas for calculating the diquark condensate and the chiral condensate. In Sec. 3, we present the effective potential for the quark propagator and then derive the Schwinger-Dyson equation as a stationary condition of the effective potential. Section 4 is the main part of this paper,

where we show the results of the numerical analysis of the Schwinger-Dyson equation. Finally, we give a summary and discussions in Sec. 5. In Appendices we summarize several intricate expressions and useful formulas.

2 Preliminary

In this section we summarize the quark propagator, the gluon propagator and the running coupling which we use in the numerical analysis. In subsection 2.1, we introduce the eight-component Majorana spinor (Nambu-Gorkov field) and give a general form of the full quark propagator as a matrix in the Nambu-Gorkov space. We obtain constraints to the full propagator from the parity and time reversal invariances. We further make several assumptions to restrict the form of the propagator. The gluon propagator with screening mass effects is shown in subsection 2.2. We also show the explicit form of the running coupling which we will use in our numerical analysis. We give formulas to calculate the quark-antiquark condensate and the diquark condensate in subsection 2.3.

2.1 Nambu-Gorkov fields and Quark propagator

Since we are interested in the phase structure of QCD including the color superconducting phase, it is convenient to use the eight-component Majorana spinor (Nambu-Gorkov field) instead of four-component Dirac spinors. The Nambu-Gorkov field is expressed as

$$\Psi = \frac{1}{\sqrt{2}} \begin{pmatrix} \psi \\ \psi^C \end{pmatrix} , \quad \psi^C = C\bar{\psi}^T , \tag{2.1}$$

where $C = i\gamma^2\gamma^0$. Here and henceforth we suppress the color and flavor indices for a while. Using the Nambu-Gorkov basis, the inverse of the free quark propagator is given by

$$iS_F^{(0)-1}(p) = \begin{pmatrix} (p_0+\mu)\gamma^0 - \vec{\gamma}\cdot\vec{p} & 0 \\ 0 & (p_0-\mu)\gamma^0 - \vec{\gamma}\cdot\vec{p} \end{pmatrix} . \tag{2.2}$$

Similarly, the full quark propagator is written in the matrix form in the Nambu-Gorkov

space as

$$S_F(p) \;=\; \begin{pmatrix} S_{F11}(p) & S_{F12}(p) \\ S_{F21}(p) & S_{F22}(p) \end{pmatrix} . \tag{2.3}$$

Four components of the above full quark propagator are not totally independent: From the relation $\psi^C = C\bar{\psi}^T$ it is shown that they satisfy

$$S_{F11}(p) = C[S_{F22}(-p)]^T C^{-1} , \tag{2.4}$$

$$S_{F21}(p) = C[S_{F21}(-p)]^T C^{-1} , \qquad S_{F12}(p) = C[S_{F12}(-p)]^T C^{-1} , \tag{2.5}$$

where ^{T} implies the transposed matrix. Furthermore, we easily find the following relations among the components of the inverse propagator[3]:

$$i\{S_F^{-1}(p)\}_{11} + i\{S_F^{-1}(p)\}_{22} \;=\; \gamma^0[i\{S_F^{-1}(p)\}_{11} + i\{S_F^{-1}(p)\}_{22}]^\dagger\gamma^0 , \tag{2.6}$$

$$i\{S_F^{-1}(p)\}_{21} \;=\; \gamma^0[i\{S_F^{-1}(p)\}_{12}]^\dagger\gamma^0 , \tag{2.7}$$

where † implies the hermitian conjugate matrix.

QCD Lagrangian at finite density is not invariant under the charge conjugation ($\mathcal{C}$) due to the existence of the chemical potential μ, while it is invariant under the time reversal ($\mathcal{T}$) and the parity ($\mathcal{P}$) transformation. Time reversal of the full quark propagator is given by

$$S_F(p^0,\vec{p}) \underset{\mathcal{T}}{\longrightarrow} \tilde{T}[S_F(p^0,-\vec{p})]^T\tilde{T} , \qquad \tilde{T} = \begin{pmatrix} T & 0 \\ 0 & T \end{pmatrix} , \quad T = i\gamma^1\gamma^3\gamma^0 . \tag{2.8}$$

Parity transformation is expressed as

$$S_F(p^0,\vec{p}) \underset{\mathcal{P}}{\longrightarrow} \Gamma^0 S_F(p^0,-\vec{p})\Gamma^0 , \qquad \Gamma^0 = \begin{pmatrix} \gamma^0 & 0 \\ 0 & -\gamma^0 \end{pmatrix} . \tag{2.9}$$

For $\mu = 0$, the charge conjugation ($\mathcal{C}$) is not broken explicitly. The charge conjugation transformation is expressed as

$$S_F(p) \underset{\mathcal{C}}{\longrightarrow} \tilde{C}[S_F(-p)]^T\tilde{C}^{-1} , \qquad \tilde{C} = \begin{pmatrix} C & 0 \\ 0 & C \end{pmatrix} . \tag{2.10}$$

According to the spinor structure the inverse full quark propagator is generally parametrized by eight bases[15]:

$$\{\ 1,\ \gamma_5,\ \gamma_0,\ \gamma_5\gamma_0,\ \vec{\gamma}\cdot\vec{p},\ \gamma_5\vec{\gamma}\cdot\vec{p},\ \gamma_0\vec{\gamma}\cdot\vec{p},\ \gamma_5\gamma_0\vec{\gamma}\cdot\vec{p}\ \} . \tag{2.11}$$

Let $\{S_F^{-1}(p)\}_{IJ}$ $(I,J=1,2)$ denote the I-J Nambu-Gorkov component of the inverse full propagator[#1]. By using the above bases, general forms of $\{S_F^{-1}(p)\}_{11}$ and $\{S_F^{-1}(p)\}_{12}$ are expressed as

$$\begin{aligned} i\{S_F^{-1}(p)\}_{11} &= -B(p) + A(p)(p_0+\mu)\gamma_0 + C(p)\vec{\gamma}\cdot\vec{p} + D(p)\gamma_0\vec{\gamma}\cdot\vec{p} \\ &\quad +\Delta^+_{(5)}(p)\gamma_5\Lambda_p^+ + \Delta^-_{(5)}(p)\gamma_5\Lambda_p^- + \Xi^+_{(5)}(p)\gamma_5\gamma_0\Lambda_p^+ + \Xi^-_{(5)}(p)\gamma_5\gamma_0\Lambda_p^- \ , \end{aligned} \tag{2.12}$$

$$\begin{aligned} i\{S_F^{-1}(p)\}_{12} &= \Delta^+(p)\gamma_5\Lambda_p^+ + \Delta^-(p)\gamma_5\Lambda_p^- + \Xi^+(p)\gamma_5\gamma_0\Lambda_p^+ + \Xi^-(p)\gamma_5\gamma_0\Lambda_p^- \\ &\quad +B_{(5)}(p) + A_{(5)}(p)\gamma_0 + C_{(5)}(p)\vec{\gamma}\cdot\vec{p} + D_{(5)}(p)\gamma_0\vec{\gamma}\cdot\vec{p}\,, \end{aligned} \tag{2.13}$$

where Λ_p^- and Λ_p^+ are the projection operators for the quark and antiquark in the massless limit:

$$\Lambda_p^{\mp} = \frac{1}{2}\left(1 \mp \frac{\gamma^0\vec{\gamma}\cdot\vec{p}}{\bar{p}}\right) . \tag{2.14}$$

It should be noticed that the above functions B, A, ..., etc. do not carry spinor indices, while they are still matrices in the color and flavor spaces. We assume here that the $O(3)$ symmetry (spatial rotation) is not broken, so that B, A, ..., etc. are functions in p_0 and $\bar{p} \equiv |\vec{p}|$. To avoid the notational complexity we write $B(p)$ instead of writing $B(p_0,\bar{p})$. In the following discussion, we often write $B(-p)$, which implies $B(-p_0,\bar{p})$.

Equations (2.4) and (2.7) relate $\{S_F^{-1}(p)\}_{22}$ and $\{S_F^{-1}(p)\}_{21}$ to $\{S_F^{-1}(p)\}_{11}$ and $\{S_F^{-1}(p)\}_{12}$, respectively. By using the notations in Eqs. (2.12) and (2.13), $\{S_F^{-1}(p)\}_{22}$ and $\{S_F^{-1}(p)\}_{21}$ are expressed as

$$\begin{aligned} i\{S_F^{-1}(p)\}_{22} &= C[i\{S_F^{-1}(-p)\}_{11}]^T C^{-1} \\ &= -[B(-p)]^T + [A(-p)]^T(p_0-\mu)\gamma_0 + [C(-p)]^T\vec{\gamma}\cdot\vec{p} + [D(-p)]^T\gamma_0\vec{\gamma}\cdot\vec{p} \\ &\quad +[\Delta^+_{(5)}(-p)]^T\gamma_5\Lambda_p^+ + [\Delta^-_{(5)}(-p)]^T\gamma_5\Lambda_p^- \\ &\quad +[\Xi^+_{(5)}(-p)]^T\gamma_5\gamma_0\Lambda_p^- + [\Xi^-_{(5)}(-p)]^T\gamma_5\gamma_0\Lambda_p^+ \ , \end{aligned} \tag{2.15}$$

$$\begin{aligned} i\{S_F^{-1}(p)\}_{21} &= \gamma_0[i\{S_F^{-1}(p)\}_{12}]^\dagger\gamma_0 \\ &= -[\Delta^-(p)]^\dagger\gamma_5\Lambda_p^+ - [\Delta^+(p)]^\dagger\gamma_5\Lambda_p^- - [\Xi^+(p)]^\dagger\gamma_5\gamma_0\Lambda_p^+ - [\Xi^-(p)]^\dagger\gamma_5\gamma_0\Lambda_p^- \\ &\quad +[B_{(5)}(p)]^\dagger + [A_{(5)}(p)]^\dagger\gamma_0 + [C_{(5)}(p)]^\dagger\vec{\gamma}\cdot\vec{p} - [D_{(5)}(p)]^\dagger\gamma_0\vec{\gamma}\cdot\vec{p}\,, \end{aligned} \tag{2.16}$$

[#1]Note that in our notation $\{S_F^{-1}\}_{IJ} \neq \{S_{FIJ}\}^{-1}$.

In the above expressions the full quark propagator include sixteen functions, which are still matrices in the color and flavor spaces. Here we obtain the constraints on these functions from Eqs. (2.5) and (2.6). First, Eq. (2.5) leads to

$$\Delta^{\pm}(p) = [\Delta^{\pm}(-p)]^T, \quad \Xi^{\pm}(p) = [\Xi^{\pm}(-p)]^T \ , \tag{2.17}$$

and

$$\begin{aligned} &B_{(5)}(p) = [B_{(5)}(-p)]^T, \quad A_{(5)}(p) = -[A_{(5)}(-p)]^T \ , \\ &C_{(5)}(p) = -[C_{(5)}(-p)]^T, \quad D_{(5)}(p) = -[D_{(5)}(-p)]^T \ . \end{aligned} \tag{2.18}$$

Second, the relation (2.6) leads to

$$\begin{aligned} &(p_0+\mu)A(p) + (p_0-\mu)A(-p) = [(p_0+\mu)A(p) + (p_0-\mu)A(-p)]^\dagger \ , \\ &B(p) + B(-p) = [B(p) + B(-p)]^\dagger \ , \qquad C(p) + C(-p) = [C(p) + C(-p)]^\dagger \ , \\ &iD(p) + iD(-p) = [iD(p) + iD(-p)]^\dagger \ , \end{aligned} \tag{2.19}$$

and

$$\begin{aligned} &i\Delta^+_{(5)}(p) + i\Delta^+_{(5)}(-p) = [i\Delta^-_{(5)}(p) + i\Delta^-_{(5)}(-p)]^\dagger \ , \\ &\Xi^+_{(5)}(p) + \Xi^-_{(5)}(-p) = [\Xi^+_{(5)}(p) + \Xi^-_{(5)}(-p)]^\dagger \ . \end{aligned} \tag{2.20}$$

Let us further constrain the forms of the functions using time reversal ($\mathcal{T}$) and parity ($\mathcal{P}$). In various analysis [2, 3, 4, 16, 17] it was shown that the most favorable condensate carries the even parity, though it was pointed in Ref. [18] that the parity violating condensate can be formed. In the present analysis, however, we use the SDE with one-gluon exchange kernel so that there exists $\mathrm{U(1)_A}$ symmetry in the system. This $\mathrm{U(1)_A}$ symmetry enables us to choose the vacuum with even parity. In such a case, the number of the functions are reduced to eight:

$$B_{(5)}(p) = A_{(5)}(p) = C_{(5)}(p) = D_{(5)}(p) = 0 \ , \tag{2.21}$$

$$\Delta^+_{(5)}(p) = \Delta^-_{(5)}(p) = \Xi^+_{(5)}(p) = \Xi^-_{(5)}(p) = 0 \ . \tag{2.22}$$

If $\mathcal{T}$ is not broken spontaneously, we obtain the following constraints for the functions allowed by $\mathcal{P}$ invariance:

$$\begin{aligned} &[A(p)]^T = A(p) \ , \quad [B(p)]^T = B(p) \ , \quad [C(p)]^T = C(p) \ , \quad [D(p)]^T = -D(p) \ , \\ &[\Delta^{\pm}(p)]^* = \Delta^{\pm}(p) \ , \quad [\Xi^{\pm}(p)]^* = -\Xi^{\pm}(p) \ . \end{aligned} \tag{2.23}$$

Now, let us consider the flavor and color structures of A, B, C, D, $\Delta^{\pm}$ and $\Xi^{\pm}$. As we discussed in the introduction, we consider that the strange quark mass is large enough to neglect the strange quark in the formation of the diquark condensate of u and d quarks. Then the color superconductivity is realized in the 2SC phase, where the color $\mathrm{SU(3)_c}$ symmetry is broken down to its subgroup $\mathrm{SU(2)_c}$. In the chiral symmetry broken (χSB) phase, on the other hand, the chiral $\mathrm{SU(2)_L \times SU(2)_R}$ symmetry is broken down to its diagonal subgroup $\mathrm{SU(2)_V}$. Functions in the full quark propagator are written to reflect these symmetry breaking structures. Here we consider the color and flavor structures in the mixed phase where both the color symmetry breaking and the chiral symmetry breaking discussed above occur simultaneously: $\mathrm{SU(3)_c \times SU(2)_L \times SU(2)_R} \to \mathrm{SU(2)_c \times SU(2)_V}$. Pure 2SC phase [$\mathrm{SU(2)_L \times SU(2)_R}$ is left unbroken] or pure χSB phase [$\mathrm{SU(3)_c}$ is left unbroken] can be realized in a certain limit of certain functions. The pure 2SC phase is realized for $B = D = \Xi^{\pm} = 0$, and the pure χSB phase for $\Delta^{\pm} = \Xi^{\pm} = 0$. Under this breaking pattern the possible color and flavor structure of the functions are given by

$$\begin{aligned} A(p),\ B(p),\ C(p),\ D(p) &\sim \delta^{ij}(\delta^{ab} - \delta^{a3}\delta^{b3}) , \quad \delta^{ij}\delta^{a3}\delta^{b3} , \\ \Delta^{\pm}(p),\ \Xi^{\pm}(p) &\sim \epsilon_{ij}\epsilon^{ab3} , \quad \delta_{ij}\epsilon^{ab3} , \end{aligned} \tag{2.24}$$

where (a, b) and (i, j) are the color and flavor indices, respectively, and we fix the direction of the color symmetry breaking to 3-direction without loss of generality. Under the transpose of color and flavor indices, the function D has to be symmetric from the symmetry breaking pattern [see Eq. (2.24)] but antisymmetric from the time reversal invariance [see Eq. (2.23)], so the function D has to vanish:

$$D(p) = 0 . \tag{2.25}$$

Next we make several approximations to the structure of the quark propagator. At zero density and zero temperature the SDE with the ladder approximation in the Landau gauge leads to the fact that the wave function renormalization of the quark is one (see, e.g., Ref. [19]). Even at high density the deviation of the wave function renormalization from one is shown to be small[6]. In addition, $A(p)\neq 1$ as well as $C(p)\neq 1$ does not imply chiral symmetry breaking. Therefore, in this paper we neglect the deviation

from one and regard $A(p) = C(p) = 1$ as an approximate solution for general μ. Furthermore, we assume that the chirality even channel in the majorana masses is dominant, and neglect the chirality odd parts:

$$\Xi^+(p) = \Xi^-(p) = 0 \ .$$

Actually, in the high density region where the chiral condensate vanishes, two quarks with same helicity, i.e., same chirality in the massless limit, condense (see, e.g., Ref. [15]). Finally, since the color and flavor structure of the diquark condensate is given by $\epsilon_{ij}\epsilon^{ab3}$, we neglect the terms proportional to $\delta_{ij}\epsilon^{ab3}$ in the function $\Delta^{\pm}$: We fix the color and flavor structures of $\Delta^{\pm}$ as

$$\Delta^{\pm}(p) \sim \epsilon_{ij}\epsilon^{ab3} \ . \tag{2.26}$$

From the above discussion the inverse full quark propagator is expressed as

$$iS_F(p)^{-1} \ = \ \begin{pmatrix} (p_0+\mu)\gamma^0 - \vec{\gamma}\cdot\vec{p} - B(p) & \Delta(p) \\ \tilde{\Delta}(p) & (p_0-\mu)\gamma^0 - \vec{\gamma}\cdot\vec{p} - B(-p) \end{pmatrix} \ , \tag{2.27}$$

where[#2]

$$\begin{aligned} \Delta(p)^{ab}_{ij} &= \epsilon_{ij}\epsilon^{ab3}\gamma_5[\Delta^+(p)\Lambda_p^+ + \Delta^-(p)\Lambda_p^-] \ , \\ \tilde{\Delta}(p)^{ab}_{ij} &= \gamma^0\Delta(p)^{\dagger ab}_{\ \ ij}\gamma^0 \\ &= -\epsilon_{ij}\epsilon^{ab3}\gamma_5[\Delta^+(p)\Lambda_p^- + \Delta^-(p)\Lambda_p^+] \ , \\ B(p)^{ab}_{ij} &= B_1(p)\delta^{ij}(\delta^{ab} - \delta^{a3}\delta^{b3}) + B_3(p)\delta^{ij}\delta^{a3}\delta^{b3} \ . \end{aligned} \tag{2.28}$$

Now the full quark propagator includes four scalar functions, $B_{1,3}$ corresponding to the Dirac masses responsible for the chiral symmetry breaking and $\Delta^{\pm}$ corresponding to the Majorana masses responsible for the color symmetry breaking. From Eq. (2.19) the Dirac masses $B_{1,3}$ obeys the following constraint:

$$\mathrm{Im}\,[B_{1,3}(p)] = -\mathrm{Im}\,[B_{1,3}(-p)] \ . \tag{2.29}$$

[#2]Note that in Eqs. (2.13), (2.16), (2.17), (2.23) and (2.24), $\Delta^{\pm}$ are still matrices in the color and flavor spaces. In Eq. (2.28) the same notations are used to express the scalar functions after factoring the color and flavor indices.

For the Majorana masses $\Delta^{\pm}(p)$ Eqs. (2.17) and (2.23) imply that they are real and even functions in p_0:

$$\Delta^{\pm}(p) = \Delta^{\pm}(-p) = \left[\Delta^{\pm}(p)\right]^* \ . \tag{2.30}$$

By taking the inverse of the expression in Eq. (2.27), the full quark propagator is given by [6]

$$-iS_F(p) \ = \ \begin{pmatrix} R_+^{-1}(p) & -\{(p_0+\mu)\gamma^0 - \vec{\gamma}\cdot\vec{p} - B(p)\}^{-1}\Delta(p)R_-^{-1}(p) \\ -\{(p_0-\mu)\gamma^0 - \vec{\gamma}\cdot\vec{p} - B(-p)\}^{-1}\tilde{\Delta}(p)R_+^{-1}(p) & R_-^{-1}(p) \end{pmatrix} , \tag{2.31}$$

where

$$\begin{aligned} R_+(p) &\equiv \{(p_0+\mu)\gamma^0 - \vec{\gamma}\cdot\vec{p} - B(p)\} - \Delta(p)\{(p_0-\mu)\gamma^0 - \vec{\gamma}\cdot\vec{p} - B(-p)\}^{-1}\tilde{\Delta}(p) \ , \\ R_-(p) &\equiv \{(p_0-\mu)\gamma^0 - \vec{\gamma}\cdot\vec{p} - B(-p)\} - \tilde{\Delta}(p)\{(p_0+\mu)\gamma^0 - \vec{\gamma}\cdot\vec{p} - B(p)\}^{-1}\Delta(p) \ . \end{aligned} \tag{2.32}$$

To use S_F in the Schwinger-Dyson equation we need explicit forms of R_+^{-1}, R_-^{-1}, and so on. We summarized them in Appendix A.

2.2 Gluon propagator and the running coupling

In dense medium gluons generally acquire Debye masses. Based on the renormalization group equation[12] and the Schwinger-Dyson equation[6, 7] in the high density region it was shown that the long range interaction mediated by magnetic gluons give the dominant contribution to the formation of the Majorana mass gap. The value of the Majorana mass gap obtained from these analyses is consistent with that derived by the models based on the instanton induced interaction [4]. In addition to the Debye masses, five gluons have Meissner masses due to the Meissner-Higgs effect when the color SU(3) is broken to its subgroup SU(2). According to the SDE analysis in the high density region[6], these masses can be neglected.

In this paper we include Debye masses in the gluon propagator through the hard dense loop approximation. On the other hand, we neglect Meissner masses. Moreover, we take the Landau gauge for the gluon propagator since it is considered to be consistent with

QCD at $\mu = 0$. (see, e.g., Ref. [20]) The explicit form of the gluon propagator which we use in this paper is given by [6]

$$\begin{aligned} D_{\mu\nu}^{AB}(k) &\equiv \delta^{AB} D_{\mu\nu}(k) \\ &= i\delta^{AB} \frac{|\vec{k}|}{|\vec{k}|^3 + \pi {M_D}^2 |k_4|/2} O_{\mu\nu}^{(1)} + i\delta^{AB} \frac{1}{(k_4)^2 + |\vec{k}|^2 + 2M_D^2} O_{\mu\nu}^{(2)} \ , \end{aligned} \tag{2.33}$$

where $k_4 = -ik_0$ and M_D is the Debye mass of the gluon. In the hard dense loop approximation this is given by [6]

$$M_D = \frac{\sqrt{N_f}}{2\pi} g(\mu)\mu \ . \tag{2.34}$$

$O_{\mu\nu}^{(i)} (i = 1, 2)$ are the polarization tensors defined by

$$O_{\mu\nu}^{(1)} = P_{\mu\nu}^{\perp} + \frac{(u\cdot k)^2}{(u\cdot k)^2 - k^2} P_{\mu\nu}^{u} \ , \qquad O_{\mu\nu}^{(2)} = -\frac{(u\cdot k)^2}{(u\cdot k)^2 - k^2} P_{\mu\nu}^{u} \ , \tag{2.35}$$

where

$$P_{\mu\nu}^{\perp} = g_{\mu\nu} - \frac{k_\mu k_\nu}{k^2} \ , \qquad P_{\mu\nu}^{u} = \frac{k_\mu k_\nu}{k^2} - \frac{k_\mu u_\nu + u_\mu k_\nu}{u\cdot k} + \frac{u_\mu u_\nu}{(u\cdot k)^2} k^2 \ . \tag{2.36}$$

Lorentz four-vector $u^\mu = (1, 0, 0, 0)$ in the gluon propagator reflects the explicit breaking of Lorentz symmetry by the existence of the chemical potential at the rest frame of the medium.

In the SDE at zero density it is important to use the running coupling since the high-energy behavior of the mass function derived from the SDE with the running coupling is consistent with that derived from the operator product expansion[19]. One of the consistent ways to include the effect of the running coupling is using the improved ladder approximation [21], in which the high-energy behavior of the running coupling is determined by the one-loop renormalization group equation derived in QCD and the low-energy behavior is suitably regularized. In the present analysis we will consider low and medium density region, so that we use the following Higashijima-Miransky type[21, 22] running coupling:

$$\alpha_s(E) = \frac{g^2(E)}{4\pi} = \frac{6\pi/(11N_c - 2N_f)}{\max(t, t_f)} \ , \tag{2.37}$$

where

$$t = \ln \frac{E}{\Lambda_{\rm qcd}} \ , \qquad t_f = \ln \frac{E_f}{\Lambda_{\rm qcd}} \ , \tag{2.38}$$

with E being the energy scale, $\Lambda_{\rm qcd}$ the characteristic scale of QCD [#3] and E_f the infrared cutoff scale introduced to regularize the infrared singularity[#4]. As we discussed in the introduction, in the present analysis we assume that the mass of the strange quark is large enough to neglect the s-quark in the formation of the diquark condensation of u and d quarks. On the other hand, it is natural to assume that the mass of s-quark is smaller than $\Lambda_{\rm qcd}$. In such a case, the effect from the s-quark should be included in the running coupling[#5]. Thus we set $N_f = 3$ and $N_c = 3$ in the running coupling (2.37). Note that the value of the running coupling in the infrared region needs to be large enough in order to involve the effect of dynamical symmetry breaking, i.e., t_f has to be small enough. Here we set $t_f = 0.5$ around which the various physical quantities for $\mu = 0$ are very stable against the change of t_f[22]. In the numerical analysis we investigate the t_f dependence of the results.

2.3 Condensates

In this subsection we give formulas to calculate the chiral condensate and the diquark condensate.

The chiral condensate is generally expressed as

$$\langle\Omega|\bar{\psi}^i_a\psi^a_i(0)|\Omega\rangle_\Lambda = -\int^\Lambda \frac{d^4p}{(2\pi)^4}{\rm tr}[S_{F11}] \ , \tag{2.39}$$

where $|\Omega\rangle$ is the ground state at nonzero density and trace is taken in the spinor, flavor and color spaces. Summations over the color index a and the flavor index i are implicitly taken in the left-hand-side of Eq. (2.39). Λ is the ultraviolet cutoff introduced to regularize the logarithmic divergence. In the actual numerical analysis we introduce two cutoffs for the temporal and spatial components of the momentum but they are expressed symbolically as Λ in this subsection. For the present form of the full quark propagator in Eq. (2.31)

[#3] Here $\Lambda_{\rm qcd}$ is determined from the infrared structure of the present analysis, while usual $\Lambda_{\rm QCD}$ is determined from the ultraviolet structure.

[#4] When we study the high density region we need to add another cutoff scale $\ln(\mu/\Lambda_{\rm qcd})$, at which the running stops. However this is neglected here because we study only the intermediate region around the phase transition point.

[#5] As we will show in the next section, $\Lambda_{\rm qcd} = 604$[MeV] in the present analysis, which is obviously larger than the s-quark mass.

this is given by

$$\begin{aligned}
&\langle\Omega|\bar{\psi}_a^i\psi_i^a(0)|\Omega\rangle_\Lambda \\
&\quad = \int^\Lambda \frac{d^4p}{i(2\pi)^4} \\
&\qquad \Big[\frac{16}{F(p,B_1,\Delta)}\Big\{\Big((p_0-\mu)^2-\bar{p}^2-\{B_1(-p)\}^2\Big)B_1(p)-\Delta^+(p)\Delta^-(p)B_1(-p)\Big\} \\
&\qquad\quad +\frac{8}{F(p,B_3,\Delta=0)}\Big((p_0-\mu)^2-\bar{p}^2-\{B_3(-p)\}^2\Big)B_3(p)\Big] \ , \qquad (2.40)
\end{aligned}$$

where F is defined as

$$\begin{aligned}
F(p,B_1,\Delta) &= [(p_0+\mu)^2-\bar{p}^2-\{B_1(p)\}^2][(p_0-\mu)^2-\bar{p}^2-\{B_1(-p)\}^2] \\
&\quad -[(p_0)^2-(\bar{p}-\mu)^2]|\Delta^+(p)|^2-[(p_0)^2-(\bar{p}+\mu)^2]|\Delta^-(p)|^2 \\
&\quad +|\Delta^+(p)|^2|\Delta^-(p)|^2+2B_1(p)B_1(-p)\Delta^+(p)\Delta^-(p) \ . \qquad (2.41)
\end{aligned}$$

For the chiral condensate of the charge conjugated quarks we obtain the following relation from Eq. (2.4):

$$\begin{aligned}
&\langle\Omega|[\bar{\psi}_C]_a^i[\psi_C]_i^a(0)|\Omega\rangle_\Lambda \\
&\quad = -\int^\Lambda \frac{d^4p}{(2\pi)^4}\mathrm{tr}[S_{F22}] = -\int^\Lambda \frac{d^4p}{(2\pi)^4}\mathrm{tr}[S_{F11}] \\
&\quad = \langle\Omega|\bar{\psi}_a^i\psi_i^a(0)|\Omega\rangle_\Lambda \ . \qquad (2.42)
\end{aligned}$$

These expressions become the following familiar form when we set $\mu = 0$, $\Delta = 0$ and $B_1 = B_3 = B$:

$$\begin{aligned}
\langle\Omega|\bar{\psi}_a^i\psi_i^a(0)|\Omega\rangle_\Lambda &= \langle\Omega|[\bar{\psi}_C]_a^i[\psi_C]_i^a(0)|\Omega\rangle_\Lambda \\
&= -4N_cN_f\int^\Lambda \frac{d^4p}{i(2\pi)^4}\frac{B(p)}{-(p_0)^2+\bar{p}^2+\{B(p)\}^2} \ , \qquad (2.43)
\end{aligned}$$

where $N_c = 3$ and $N_f = 2$.

The diquark condensate is generally expressed as

$$\langle\Omega|(\epsilon^{ij}\epsilon_{ab3})[\psi^T]_i^aC\gamma_5\psi_j^b(0)|\Omega\rangle_\Lambda = -\int^\Lambda \frac{d^4p}{(2\pi)^4}\mathrm{tr}[\epsilon^{(c)}\epsilon^{(f)}S_{F12}\gamma_5] \ , \qquad (2.44)$$

where $\epsilon^{(c)}$ and $\epsilon^{(f)}$ are antisymmetric matrices in the color and flavor spaces, respectively:

$$\{\epsilon^{(c)}\}^{ab} = \epsilon^{ab3} \ , \qquad \{\epsilon^{(f)}\}_{ij} = \epsilon_{ij} \ . \qquad (2.45)$$

In the present approximation the diquark condensate is given by

$$\begin{aligned}
&\langle\Omega|(\epsilon^{ij}\epsilon_{ab3})[\psi^T]_i^a C\gamma_5\psi_j^b(0)|\Omega\rangle_\Lambda \\
&\quad = \int^\Lambda \frac{d^4p}{i(2\pi)^4}\frac{8}{F(p,B_1,\Delta)}\Big[\Big\{(p_0)^2-(\bar{p}-\mu)^2-\{\Delta^-(p)\}^2-|B_1(p)|^2\Big\}\Delta^+(p) \\
&\qquad\qquad +\Big\{(p_0)^2-(\bar{p}+\mu)^2-\{\Delta^+(p)\}^2-|B_1(p)|^2\Big\}\Delta^-(p)\Big] \ .
\end{aligned} \tag{2.46}$$

Using the time reversal invariance [see Eq. (2.8)], we obtain

$$\begin{aligned}
&\langle\Omega|(\epsilon^{ij}\epsilon_{ab3})[\psi_C^T]_i^a C\gamma_5[\psi_C]_j^b(0)|\Omega\rangle_\Lambda \\
&\quad = -\int^\Lambda \frac{d^4p}{(2\pi)^4}\mathrm{tr}[\epsilon^{(c)}\epsilon^{(f)}S_{F21}\gamma_5] = \int^\Lambda \frac{d^4p}{(2\pi)^4}\mathrm{tr}[\epsilon^{(c)}\epsilon^{(f)}S_{F12}\gamma_5] \\
&\quad = -\langle\Omega|[\psi^T]_i^a C\gamma_5\psi_j^b(0)|\Omega\rangle_\Lambda \ .
\end{aligned} \tag{2.47}$$

We note that the parity invariance existing in the present analysis leads to the vanishing parity violating condensate:

$$\langle\Omega|(\epsilon^{ij}\epsilon_{ab3})[\psi^T]_i^a C\psi_j^b(0)|\Omega\rangle_\Lambda = -\int^\Lambda \frac{d^4p}{(2\pi)^4}\mathrm{tr}[\epsilon^{(c)}\epsilon^{(f)}S_{F12}] = 0 \ . \tag{2.48}$$

In the improved ladder approximation at zero density the high-energy behavior of the mass function is consistent with that derived by the operator product expansion (OPE). The chiral condensate calculated by using the mass function was shown to obey the renormalization group evolution derived by the OPE (see, e.g., Refs. [19]). Then, we identify the condensates, which are calculated with cutoff Λ, with those renormalized at the scale Λ in QCD. So we scale them to the condensates at 1 GeV using the leading renormalization group formulas. The relation between the chiral condensate at the scale Λ and that at the scale E is given by

$$\langle\Omega|\bar{\psi}_a^i\psi_i^a(0)|\Omega\rangle_E = \left[\frac{\ln E/\Lambda_{\rm qcd}}{\ln\Lambda/\Lambda_{\rm qcd}}\right]^\kappa \langle\Omega|\bar{\psi}_a^i\psi_i^a(0)|\Omega\rangle_\Lambda \ , \tag{2.49}$$

where

$$\kappa = \frac{9C_2(F)}{11N_c-2N_f} = \frac{9}{11N_c-2N_f}\frac{N_c^2-1}{2N_c} \ . \tag{2.50}$$

Noting that the attractive force between two quarks in $\bar{\mathbf{3}}$ channel by the one-gluon exchange is one half of that between quark and antiquark in the singlet channel, we immediately obtain the following relation between the diquark condensate at the scale Λ and

that at the scale E:

$$\langle\Omega|(\epsilon^{ij}\epsilon_{ab3})[\psi^T]_i^a C\psi_j^b(0)|\Omega\rangle_E = \left[\frac{\ln E/\Lambda_{\rm qcd}}{\ln \Lambda/\Lambda_{\rm qcd}}\right]^{\kappa/2}\langle\Omega|(\epsilon^{ij}\epsilon_{ab3})[\psi^T]_i^a C\psi_j^b(0)|\Omega\rangle_\Lambda \ . \tag{2.51}$$

3 Effective potential and Schwinger-Dyson equation

In this section we present the effective potential for the quark propagator and then derive the Schwinger-Dyson equation (SDE) as a stationary condition of the effective potential.

The effective action for the full quark propagator S_F is given by [23]

$$\Gamma[S_F] \ = \ \frac{1}{2}\Big(-i{\rm TrLn}(S_F^{-1}) - i{\rm Tr}({S_F^{(0)}}^{-1}S_F) - i\Gamma_{\rm 2PI}[S_F]\Big) \ , \tag{3.1}$$

where Tr and Ln are taken for all the spaces and $\Gamma_{\rm 2PI}[S_F]$ stands for the contributions from the two-particle irreducible (with respect to the quark line) diagrams. The factor one-half in front appears since we are using the eight-component Nambu-Gorkov spinor basis. In the high density region the one-gluon exchange approximation is valid since the coupling is weak. In the present analysis we extrapolate this approximation to the intermediate density and include only the contribution from the one-gluon exchange diagram in $\Gamma_{\rm 2PI}[S_F]$:

$$\Gamma_{\rm 2PI}[S_F] = -\frac{1}{2}{\rm Tr}(S_F\cdot ig\Gamma_A^\mu\cdot S_F\cdot ig\Gamma_B^\nu\cdot D_{\mu\nu}^{AB}) \ , \tag{3.2}$$

where Γ_A^μ is the quark-gluon vertex in the Nambu-Gorkov basis defined as

$$\Gamma_A^\mu = \begin{pmatrix} \gamma^\mu T_A & 0 \\ 0 & -\gamma^\nu (T_A)^T \end{pmatrix} \ . \tag{3.3}$$

From the effective action (3.1), the effective potential in the momentum space is written as

$$V[S_F] \ = \ -\Gamma[S_F]/\int d^4x$$

$$
\begin{aligned}
&= \frac{1}{2}\int \frac{d^4p}{i(2\pi)^4}\Big(\ln\,\det\{S_F(p)\} - \mathrm{tr}\{S_F^{(0)-1}(p)S_F(p)\}\Big) \\
&\quad + \frac{1}{2}\int \frac{d^4p}{i(2\pi)^4}\int \frac{d^4q}{i(2\pi)^4}\frac{1}{2}\mathrm{tr}\{S_F(p)\cdot ig\Gamma_A^\mu \cdot S_F(q)\cdot ig\Gamma_B^\nu\}\cdot iD_{\mu\nu}^{AB}(p-q)\ ,
\end{aligned}
\tag{3.4}
$$

where ln, det and tr are taken in the spinor, color and flavor spaces. The SDE is obtained as the stationary condition of the effective potential ($\delta V[S_F]/\delta S_F = 0$):

$$
S_F^{-1} \;=\; {S_F^{(0)}}^{-1} - (ig\Gamma_A^\mu \cdot S_F \cdot ig\Gamma_B^\nu)\cdot D_{\mu\nu}^{AB}\ . \tag{3.5}
$$

In principle, Eq. (3.5) leads to the coupled equations for seven functions [B, A, C, $\Delta^\pm$ and $\Xi^\pm$ in Eqs. (2.12)-(2.16)] in the quark propagator, which are still matrices in the color and flavor spaces. As we discussed in subsection 2.1, we assume that $A = C = 1$ and $\Xi^\pm = 0$ are the approximate solutions of the equations. Furthermore, in the present pattern of the symmetry breaking we take the color and flavor structures of the Dirac and Majonara masses as shown in Eq. (2.28). As a result, the above SDE (3.5) leads to four coupled equations for four scalar functions $B_{1,3}$ and $\Delta^\pm$. These are given by

$$
B_1(p) \;=\; \int \frac{d^4q}{i(2\pi)^4}\frac{1}{2}\pi\alpha_s D_{\mu\nu}(q-p)\mathrm{tr}[\gamma^\mu T^A S_{F11}(q)\gamma^\nu T^A \delta_1^{(c)}]\ , \tag{3.6}
$$

$$
B_3(p) \;=\; \int \frac{d^4q}{i(2\pi)^4}\pi\alpha_s D_{\mu\nu}(q-p)\mathrm{tr}[\gamma^\mu T^A S_{F11}(q)\gamma^\nu T^A \delta_3^{(c)}]\ , \tag{3.7}
$$

$$
\Delta^-(p) \;=\; \int \frac{d^4q}{i(2\pi)^4}\frac{1}{2}\pi\alpha_s D_{\mu\nu}(q-p)\mathrm{tr}[\gamma^\mu T^A S_{F12}(q)\gamma^\nu (T^A)^T \Lambda_p^- \gamma_5 \epsilon^{(c)}\epsilon^{(f)}]\ , \tag{3.8}
$$

$$
\Delta^+(p) \;=\; \int \frac{d^4q}{i(2\pi)^4}\frac{1}{2}\pi\alpha_s D_{\mu\nu}(q-p)\mathrm{tr}[\gamma^\mu T^A S_{F12}(q)\gamma^\nu (T^A)^T \Lambda_p^+ \gamma_5 \epsilon^{(c)}\epsilon^{(f)}]\ , \tag{3.9}
$$

where

$$
\{\delta_1^{(c)}\}^{ab} = \delta^{ab} - \delta^{a3}\delta^{b3}\ , \qquad\qquad \{\delta_3^{(c)}\}^{ab} = \delta^{a3}\delta^{b3}\ . \tag{3.10}
$$

and the traces are taken in the spinor, flavor and color spaces. $\alpha_s = \alpha_s(E)$ in the right-hand-sides of Eq. (3.6)$-$(3.9) is the running coupling defined in Eq. (2.37) where we take E as

$$
E^2 = -p^2 - q^2\ . \tag{3.11}
$$

The graphycal representations of these gap equations are shown in Fig. 1 and the explicit forms of these SDE's are given in Appendix A.

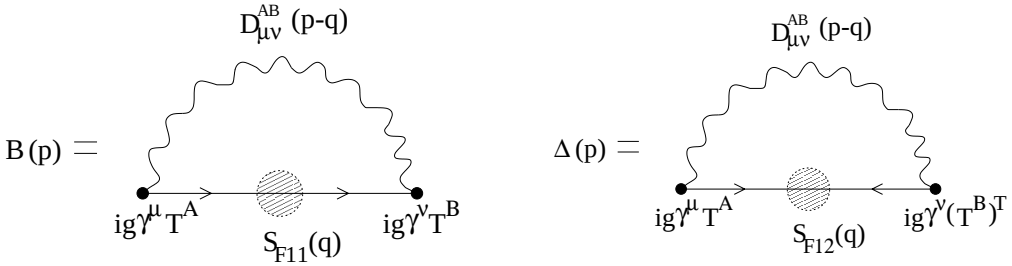

Figure 1: Graphical representations of the gap equations.

As we show in Eq. (2.30), the Majonara masses $\Delta^{\pm}(p)$ are real and even functions in p_0, while in general the Dirac masses $B_{1,3}(p)$ are complex functions. Equation (2.29) is the constraint to the imaginary part, while no constraint is obtained for the real part from general considerations. However, as was done in Ref. [24, 25] for the case of $\Delta^{\pm} = 0$, the structure of the SDE leads to a natural constraint to the real part of the Dirac masses $B_{1,3}(p)$. This is obtained as follows: Let us take the complex conjugate of the SDE's for $B_{1,3}$ in Eqs. (A.4) and (A.5). By using the fact that the kernel K_0 and the Majorana masses $\Delta^{\pm}$ are real functions, it is easily shown that the combination $\{B_1^*(p), B_3^*(p)\}$ satisfies the same coupled equations as $\{B_1(p^*), B_3(p^*)\}$ does. Since $p^{\mu *} = (p^{0*}, \vec{p}) = (-ip_4, \vec{p}) = (-p^0, \vec{p})$, this means that $\{B_1^*(p), B_3^*(p)\}$ satisfies the same coupled equations as $\{B_1(-p), B_3(-p)\}$ does. Thus these two combinations are equal to each other up to sign, $\{B_1^*(p), B_3^*(p)\} = \{B_1(-p), B_3(-p)\}$ or $\{B_1^*(p), B_3^*(p)\} = -\{B_1(-p), B_3(-p)\}$. Since the general consideration (2.29) implies that imaginary parts of $B_1(p)$ and $B_3(p)$ are odd functions in p^0, the above argument implies that the real parts are even functions in p^0:

$$B_{1,3}(-p) = B_{1,3}^*(p) \ . \tag{3.12}$$

Using the above properties for $B_{1,3}$ and those for $\Delta^{\pm}$ in Eq. (2.30), we can always restrict the integration over the temporal component of the momentum, $p_4 = -ip^0$, to its positive region.

Substituting the solution of Eq. (3.5) into Eq. (3.4) we obtain the effective potential at the vacuum, i.e., at the stationary point. Since the effective potential itself is divergent, we subtract the effective potential at the trivial vacuum:

$$\begin{aligned} & \bar{V}_{\rm sol}[\Delta^+, \Delta^-, B_1, B_3] \\ \equiv \ & V[\Delta^+, \Delta^-, B_1, B_3] - V[0, 0, 0, 0] \end{aligned}$$

$$
\begin{aligned}
= & -\int \frac{d^4p}{i(2\pi)^4} 2\Big[2\ln\Big(\frac{F(p,B_1,\Delta)}{[(p_0+\mu)^2-\bar{p}^2][(p_0-\mu)^2-\bar{p}^2]} \Big) \\
& \qquad + \ln\Big(\frac{F(p,B_3,0)}{[(p_0+\mu)^2-\bar{p}^2][(p_0-\mu)^2-\bar{p}^2]} \Big) \Big] \\
& -\int \frac{d^4p}{i(2\pi)^4} 2\Big[\frac{2}{F(p,B_1,\Delta)} \Big\{ [(p_0-\mu)^2-\bar{p}^2-\{B_1(-p)\}^2][(p_0+\mu)^2-\bar{p}^2] \\
& \qquad\qquad + [(p_0+\mu)^2-\bar{p}^2-\{B_1(p)\}^2][(p_0-\mu)^2-\bar{p}^2] \\
& \qquad\qquad - [(p_0)^2-(\bar{p}+\mu)^2]|\Delta^-|^2 - [(p_0)^2-(\bar{p}-\mu)^2]|\Delta^+|^2 \Big\} \\
& \qquad + \frac{1}{F(p,B_3,0)} \Big\{ [(p_0-\mu)^2-\bar{p}^2-\{B_3(-p)\}^2][(p_0+\mu)^2-\bar{p}^2] \\
& \qquad\qquad + [(p_0+\mu)^2-\bar{p}^2-\{B_3(p)\}^2][(p_0-\mu)^2-\bar{p}^2] \Big\} \\
& \qquad\qquad -6 \Big] \, , \qquad (3.13)
\end{aligned}
$$

where F is defined in Eq. (2.41). The value of the effective potential in Eq. (3.13) is understood as the energy density of the solution. So the true vacuum should be determined by evaluating the value of the effective potential. Smaller the value of $\bar{V}_{\rm sol}$ for a solution is, more stable the vacuum corresponding to the solution is.

4 Numerical analysis

In this section we show the results from our numerical analysis for $0.2 \leq \mu/\Lambda_{\rm qcd} \leq 1.0$. Parameters necessary to perform the numerical analysis are $\Lambda_{\rm qcd}$ and the infrared cutoff parameter t_f in the running coupling. $\Lambda_{\rm qcd}$ is the unit of the energy scale in our numerical analysis, and it is determined by calculating the pion decay constant f_π for fixed t_f in the zero density through the Pagels-Stokar formula [26]:

$$
f_\pi^2 = \frac{N_c}{4\pi^2} \int dp_E^2 p_E^2 \frac{B(p)\Big(B(p) - \frac{p_E^2}{2}\frac{\partial B(p)}{\partial p_E^2} \Big)}{p_E^2 + B^2(p)} \, . \qquad (4.1)
$$

We use $f_\pi = 88$ MeV in the chiral limit[27] as an input. For $\mu = 0$ the dependence of the physical quantities on t_f are shown to be small around $t_f = 0.5$ [22]. Then for a while, we fix $t_f = 0.5$ for general μ. From these inputs we get $\Lambda_{\rm qcd} = 604$ MeV. Later in this section we study the t_f dependence of our results.

We introduce the framework of our numerical analysis in subsection 4.1. Then we show the solutions for the Majorana masses (Δ^- and Δ^+) with fixing $B_{1,3} = 0$ in subsection 4.2.

We show the solutions for the Dirac mass ($B_{1,3}$) with $\Delta^{\pm} = 0$ in subsection 4.3. Finally, in subsection 4.4, we study the phase transition from the hadronic phase to the color superconducting phase.

4.1 Framework of the numerical analysis

In this subsection we summarize the framework of our numerical analysis. First, as we discussed below Eq. (3.12), we note that it is always possible to restrict the p_4-integral ($p_4 = -ip_0$) to its positive region from the properties in Eqs. (2.30) and (3.12). To solve the SDE's numerically we transform the variables p_4 and $\bar{p} = |\vec{p}|$ into new variables U and X. For these transformations we use the density-independent transformations in the low density region ($\mu < \mu_0$) and the density-dependent transformations in the medium density region ($\mu \geq \mu_0$), where μ_0 will be determined later in subsection 4.2. In the low density region where the chiral condensate is formed, the characteristic scale of the system is $\Lambda_{\rm qcd}$. The dynamical information mainly comes from the region $p_4,\ \bar{p} \sim \Lambda_{\rm qcd}$. On the other hand, in the high density region where the diquark condensate is formed, the chemical potential μ in addition to $\Lambda_{\rm qcd}$ gives an important scale: The dynamically important region is $p_4 \sim \Lambda_{\rm qcd}$ and $\bar{p} \sim \mu$. Therefore we adopt the following transformations:

$$p_4 = \Lambda_{\rm qcd} \cdot \exp(U)\ , \qquad \bar{p} = \Lambda_{\rm qcd} \cdot \exp(X)\ , \qquad \text{for} \quad \mu < \mu_0\ , \tag{4.2}$$

$$p_4 = 3\mu \cdot \exp(U)\ , \qquad \bar{p} = 3\mu \cdot \exp(X)\ , \qquad \text{for} \quad \mu \geq \mu_0\ . \tag{4.3}$$

By the above transformations the integrations over p_4 and $\bar{p}$ in the interval $[0, \infty]$ are converted into those over U and X in the interval $[-\infty, \infty]$. In the numerical integration we introduce the ultraviolet (UV) and the infrared (IR) cutoffs for U and X:

$$U \in [\Lambda_{IR}, \Lambda_{UV}]\ , \qquad X \in [\lambda_{IR}, \lambda_{UV}]\ . \tag{4.4}$$

We divide U and X evenly into N_U and N_X points, respectively:

$$\begin{aligned} U[I] &= \Lambda_{IR} + \Delta U \cdot I, \quad I = 0, 1, \cdots, N_U - 1, \\ X[J] &= \lambda_{IR} + \Delta X \cdot J, \quad J = 0, 1, \cdots, N_X - 1, \end{aligned} \tag{4.5}$$

where

$$\Delta U = \frac{\Lambda_{UV} - \Lambda_{IR}}{N_U - 1}, \qquad \Delta X = \frac{\lambda_{UV} - \lambda_{IR}}{N_X - 1}. \tag{4.6}$$

The integrations over p_4 and $\bar{p}$ are thus replaced with the following summations:

$$\int dp_4 \to \Delta U \sum_I e^{U[I]}, \qquad \int d\bar{p} \to \Delta X \sum_J e^{X[J]}. \tag{4.7}$$

In the present analysis, for the UV and IR cutoffs we use

$$p_4: \quad (\Lambda_{IR}, \Lambda_{UV}) = (-12.5, 2.5)\ , \qquad \bar{p}: \quad (\lambda_{IR}, \lambda_{UV}) = (-3.5, 2.5)\ . \tag{4.8}$$

The validity of these choices will be checked later.

We solve the SDE's by an iteration method. Starting from a set of trial functions, we update the mass functions by the SDE:

$$\left\{B_{1,3\mathrm{old}}\ ,\ \Delta^{\pm}_{\mathrm{old}}\right\} \Rightarrow \boxed{\text{Right-hand sides of SDE's (3.6)-(3.9)}} \Rightarrow \left\{B_{1,3\mathrm{new}}\ ,\ \Delta^{\pm}_{\mathrm{new}}\right\}\ . \tag{4.9}$$

Then we stop the iteration if the following convergence condition is satisfied:

$$\begin{aligned}
\varepsilon\Lambda^6_{\mathrm{qcd}} &> \int \frac{d^4p}{(2\pi)^4}\frac{1}{4}\mathrm{tr}\left[\left(\frac{\delta V}{\delta[S_F(p)]}\right)^{\dagger}\left(\frac{\delta V}{\delta[S_F(p)]}\right)\right] \\
&= \int \frac{d^4p}{(2\pi)^4}\Big\{2|B_{1\mathrm{old}}(p) - B_{1\mathrm{new}}(p)|^2 + |B_{3\mathrm{old}}(p) - B_{3\mathrm{new}}(p)|^2 \\
&\qquad +2|\Delta^+_{\mathrm{old}}(p) - \Delta^+_{\mathrm{new}}(p)|^2 + 2|\Delta^-_{\mathrm{old}}(p) - \Delta^-_{\mathrm{new}}(p)|^2\Big\},
\end{aligned} \tag{4.10}$$

with suitably small ε. In the present analysis we set $\varepsilon = 10^{-10}$.

4.2 $B = 0$, $\Delta \neq 0$ solution

In this subsection we solve the SDE's numerically with fixing the Dirac masses to zero ($B_1 = B_3 = 0$). The initial trial functions used here are

$$\begin{aligned}
&B_1(p) = B_3(p) = 0\ , \\
&\Delta^+(p) = 0\ , \\
&\Delta^-(p) = \Lambda_{\mathrm{qcd}}\ .
\end{aligned} \tag{4.11}$$

In this case the outputs become $B_{1,3}(p) = 0, \Delta^{\pm}(p) \neq 0$ for all μ. We call this solution the color symmetry breaking (CSB) solution.

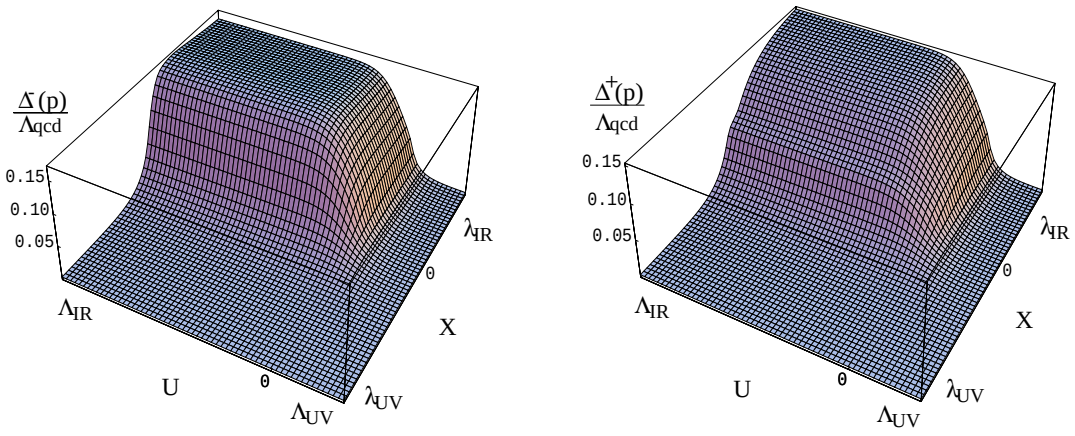

Figure 2: Momentum dependences of Majorana mass functions $\Delta^-(p)/\Lambda_{\rm qcd}$ and $\Delta^+(p)/\Lambda_{\rm qcd}$ at $\mu/\Lambda_{\rm qcd} = 0.70$.

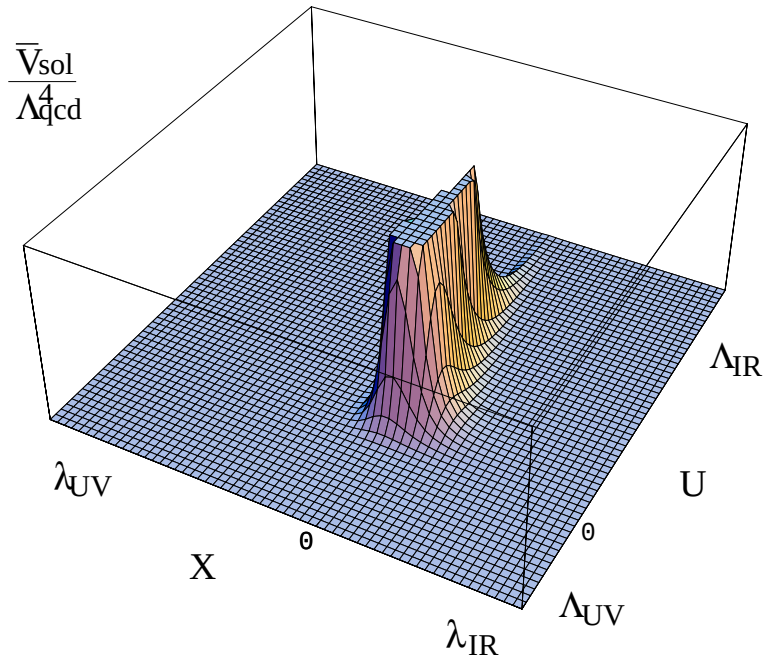

Figure 3: Integrand of $\bar{V}_{\rm sol}/\Lambda_{\rm qcd}^4$ at $\mu/\Lambda_{\rm qcd} = 0.70$. The upper 9/10 of the figure is clipped.

To check the validity of the UV and IR cutoffs in Eq. (4.8) we show the solutions $\Delta^{\mp}(p)$ and the integrand of $\bar{V}_{\rm sol}$ at $\mu/\Lambda_{\rm qcd} = 0.70$ in Figs. 2 and 3, respectively. Figure 2 shows that both Δ^- and Δ^+ become small in the UV region of p_4 as well as that of $\bar{p}$. It

was shown in, e.g., Ref. [6] that Δ^+ is very small compared with Δ^- in the high density region. In the medium density region, however, Fig. 2 shows that Δ^+ is of the same order as Δ^-. From Fig. 3 we see that the dominant contribution to the effective potential lies within the integration range. These figures imply that the choices of the ranges in Eq. (4.8) are enough at $\mu/\Lambda_{\rm qcd} = 0.70$. We perform similar analysis for all the cases we study in this paper, and confirm that the choices of the ranges in Eq. (4.8) are enough for the present purpose.

Next we show the dependence of the results on the size of descretization. We show typical values of $|\bar{V}_{\rm sol}|^{1/4}/\Lambda_{\rm qcd} \cdot {\rm sgn}[\bar{\rm V}_{\rm sol}]$[#6] in Fig. 4 and $-\langle\psi\psi\rangle_{1GeV}^{1/3}/\Lambda_{\rm qcd}$ in Fig. 5 for four choices of the size of descretization, (N_U, N_X)=(30,30), (40,40), (50,50) and (60,60). To obtain $\langle\psi\psi\rangle_{1GeV}$ we used Eq. (2.51) with

$$\Lambda^2 = \Lambda_{qcd}^2[\exp(2\Lambda_{UV}) + \exp(2\lambda_{UV})] \ , \qquad \text{for} \quad \mu < \mu_0 \ , \tag{4.12}$$

$$\Lambda^2 = 9\mu^2[\exp(2\Lambda_{UV}) + \exp(2\lambda_{UV})] \ , \qquad \text{for} \quad \mu \geq \mu_0 \ . \tag{4.13}$$

These figures show that the choice (N_U, N_X)=(60,60) is large enough for the present purpose.

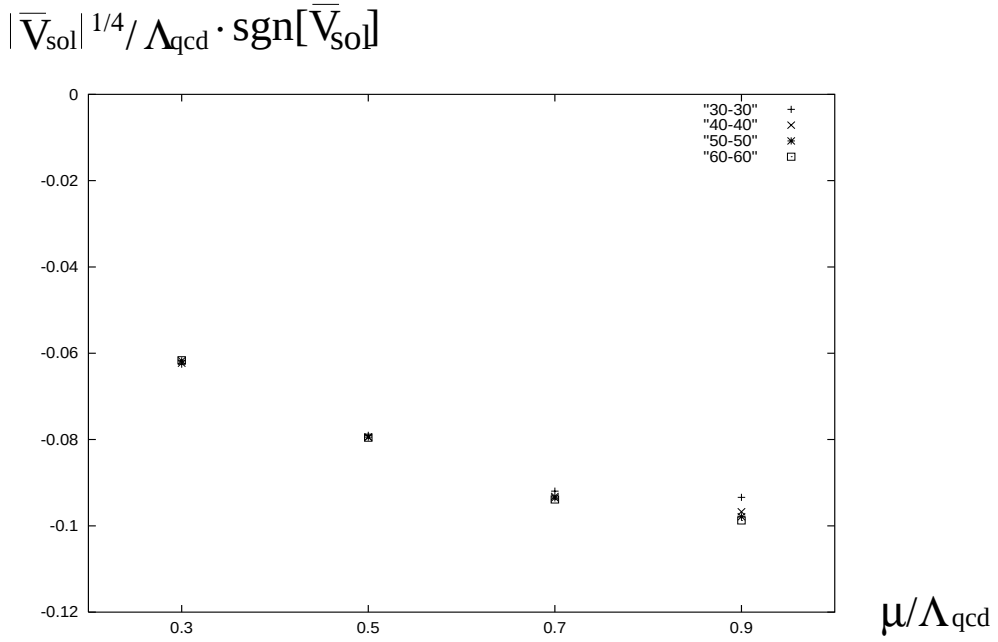

Figure 4: Typical values of $|\bar{V}_{\rm sol}|^{1/4}/\Lambda_{\rm qcd} \cdot {\rm sgn}[\bar{\rm V}_{\rm sol}]$ for four sizes of descretization, (N_U, N_X)=(30,30), (40,40), (50,50) and (60,60).

[#6] ${\rm sgn}[\bar{V}_{\rm sol}] = 1$ for $\bar{V}_{\rm sol} \geq 0$, and -1 for $\bar{V}_{\rm sol} < 0$.

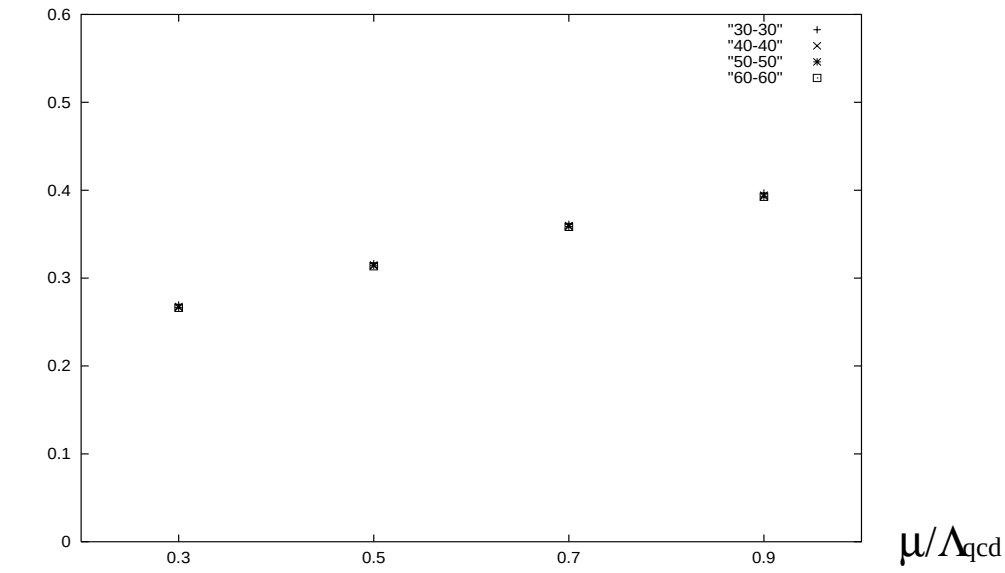

Figure 5: Typical values of $-\langle\psi\psi\rangle_{1GeV}^{1/3}/\Lambda_{\rm qcd}$ for four different sizes of descritization (N_U, N_X)=$(30,30)$, $(40,40)$, $(50,50)$ and $(60,60)$.

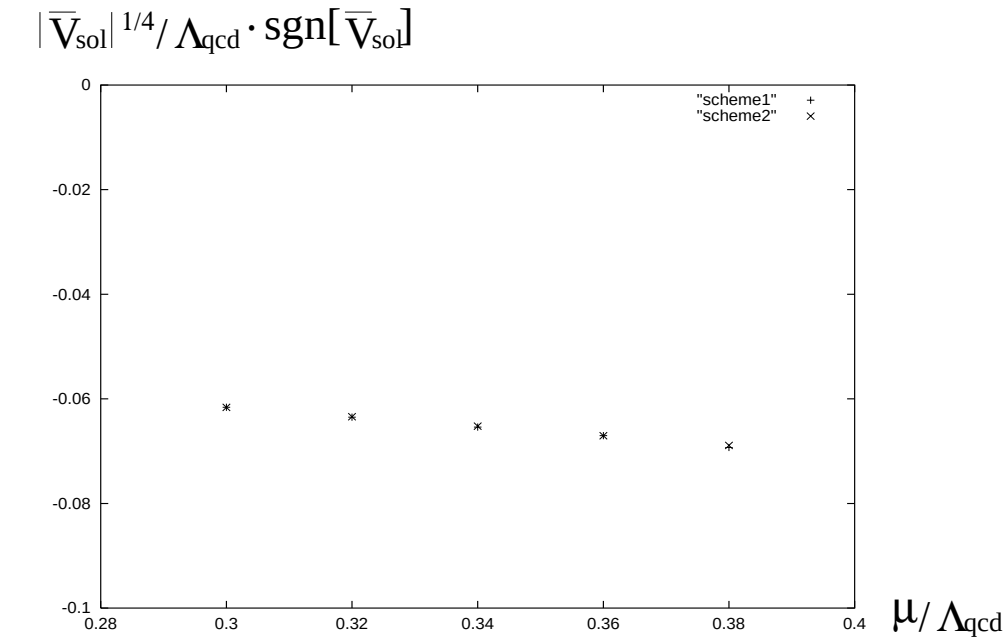

Figure 6: Typical values of $|\bar{V}_{\rm sol}|^{1/4}/\Lambda_{\rm qcd}\cdot{\rm sgn}[\bar{\rm V}_{\rm sol}]$ in two different schemes of descritization for $0.30 \le \mu/\Lambda_{\rm qcd} \le 0.38$. "scheme 1" implies that Eq. (4.2) is used and "scheme 2" implies that Eq. (4.3) is used.

Let us next check that two schemes of the descritization in Eqs. (4.2) and (4.3) are

smoothly connected with each other. For this purpose we calculate the value of $\bar{V}_{\rm sol}$ for several values of μ in $0.30 \leq \mu/\Lambda_{\rm qcd} \leq 0.38$ in two schemes. We show the results in Fig. 6. This clearly shows that two schemes are smoothly connected with each other around $\mu_0/\Lambda_{\rm qcd} = 1/3$. Thus in the following analysis we fix $\mu_0/\Lambda_{\rm qcd} = 1/3$.

Now, we show the resultant values of the diquark condensate in Fig. 7, where we used Eq. (2.51) to obtain $\langle\psi\psi\rangle_{\rm 1GeV}$. Figure 7 shows that the value is in the range of $\langle\psi\psi\rangle_{\rm 1GeV} \simeq -(150\,{\rm MeV})^3 \sim -(250\,{\rm MeV})^3$, which is comparable to the value of the chiral condensate for $\mu = 0$: $\langle\bar{\psi}\psi\rangle_{\rm 1GeV} = -(225 \pm 25\,{\rm MeV})^3$ [28]. Furthermore, this figure shows that there exists the diquark condensate for all μ we studied.

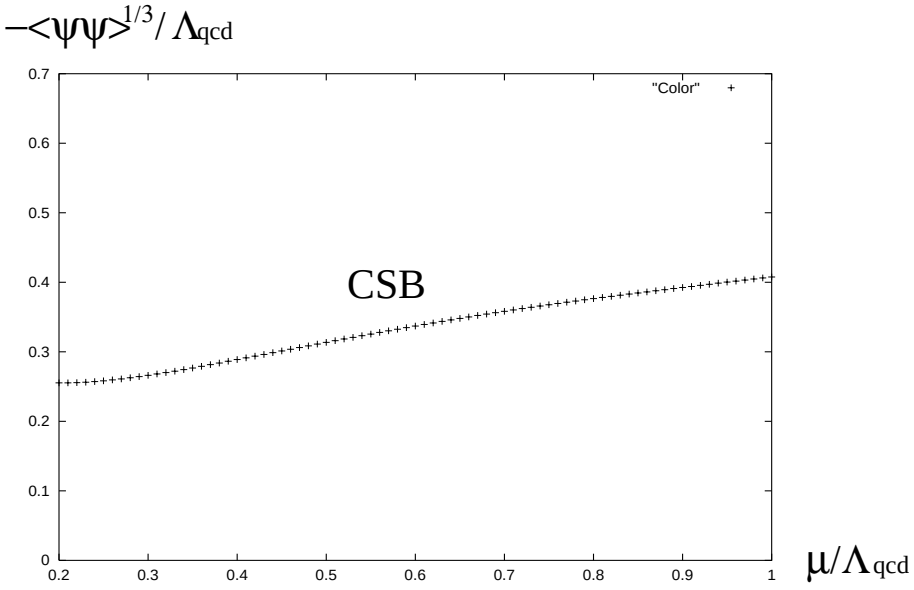

Figure 7: Chemical potential dependence of $-\langle\psi\psi\rangle^{1/3}_{1GeV}/\Lambda_{\rm qcd}$ for $0.2 \leq \mu/\Lambda_{\rm qcd} \leq 1.0$.

As we discussed in section 3, the true vacuum is determined by evaluating the value of the effective potential at the solution. We show the chemical potential dependence of $|\bar{V}_{\rm sol}|^{1/4}/\Lambda_{\rm qcd} \cdot {\rm sgn}[\bar{\rm V}_{\rm sol}]$ in Fig. 8. This figure shows that the value of the effective potential is always negative, which implies that the CSB vacuum is always more stable than the trivial vacuum with $B = \Delta = 0$. This is consistent with the result shown in Ref. [9], where the SDE was converted into the algebraic equation by using the confining model gluon propagator.

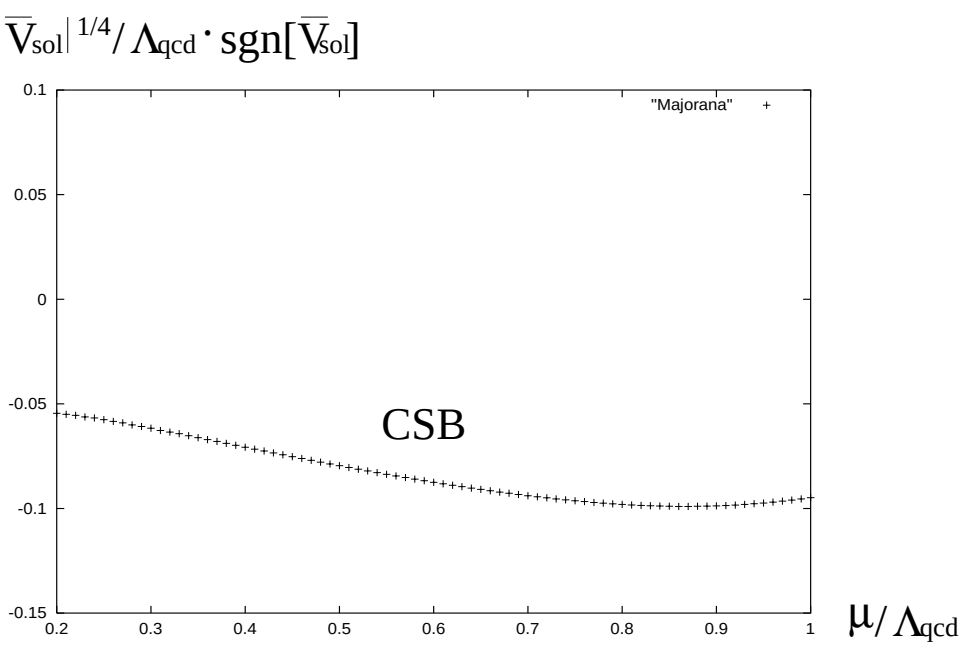

Figure 8: Chemical potential dependence of $|\bar{V}_{\rm sol}|^{1/4}/\Lambda_{\rm qcd} \cdot {\rm sgn}[\bar{\rm V}_{\rm sol}]$ for $0.2 \leq \mu/\Lambda_{\rm qcd} \leq 1.0$.

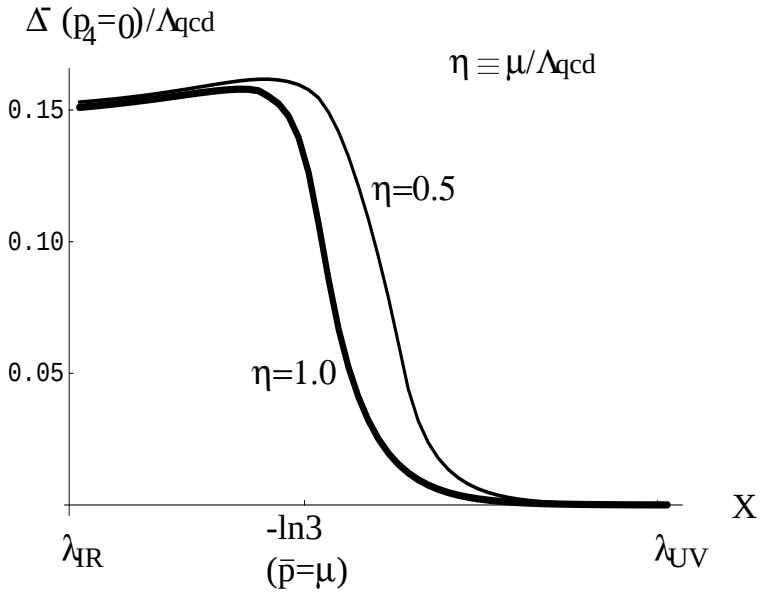

Figure 9 : $\bar{p}$-dependence of $\Delta^-(p)/\Lambda_{\rm qcd}$ at $p_4 = 0$ for $\eta \equiv \mu/\Lambda_{\rm qcd} = 0.5$ and 1.0.

Next we show the $\bar{p}$-dependence of $\Delta^-(p_4 = 0, \bar{p})/\Lambda_{\rm qcd}$ at $\mu/\Lambda_{\rm qcd} = 0.5$ and 1.0 in Fig. 9 and the p_4-dependence of $\Delta^-(p_4, \bar{p} = \mu)/\Lambda_{\rm qcd}$ in Fig. 10. These figures show that

the entire scale of the mass function becomes small when we increase μ. From Fig. 9 we see that Δ^- has a peak around $\bar{p} = \mu$ ($X = -\ln 3 \cong -1.1$). However this peak is not so sharp, and it implies that the effects of the quarks away from the Fermi surface are important in the medium density region.

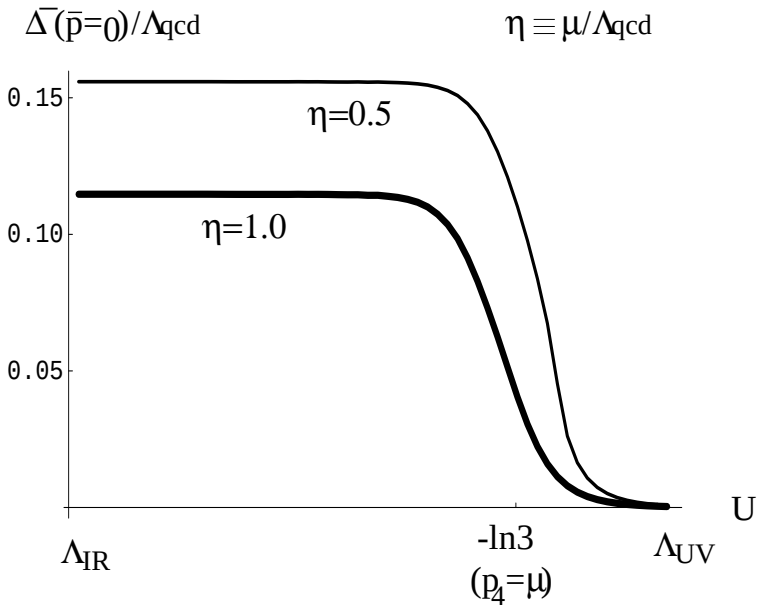

Figure 10 : p_4-dependence of $\Delta^-(p)/\Lambda_{\rm qcd}$ at $\bar{p} = \mu$ for $\eta \equiv \mu/\Lambda_{\rm qcd} =$ 0.5 and 1.0.

4.3 $B \neq 0$, $\Delta = 0$ solution

In this subsection we solve the SDE's numerically with fixing the Majorana masses to zero ($\Delta^{\pm}(p) = 0$). The initial trial functions used here are

$$\begin{aligned} B_1(p) &= \Lambda_{\rm qcd} \ , \\ B_3(p) &= 0 \ , \\ \Delta^+(p) &= \Delta^-(p) = 0 \ . \end{aligned} \tag{4.14}$$

In this case outputs become $B_1(p) = B_3(p)$, $\Delta^{\pm}(p) = 0$ for all μ. We obtain $B_{1,3}(p) \neq 0$ for small μ, and $B_{1,3}(p) = 0$ for large μ. We call the former solution the chiral symmetry breaking (χSB) solution.

In Fig. 11 we show the solutions Re$[B_1(p)]$ and Im$[B_1(p)]$ (or equivalently Re$[B_3(p)]$ and Im$[B_3(p)]$) at $\mu/\Lambda_{\rm qcd} = 0.30$. This figure shows that both the real part and the imaginary part become small above $\Lambda_{\rm qcd}$ (U, X=0), and that the imaginary part has a peak around $p_4 = \Lambda_{\rm qcd}$ (U=0). These structures are consistent with those obtained in Ref. [25].

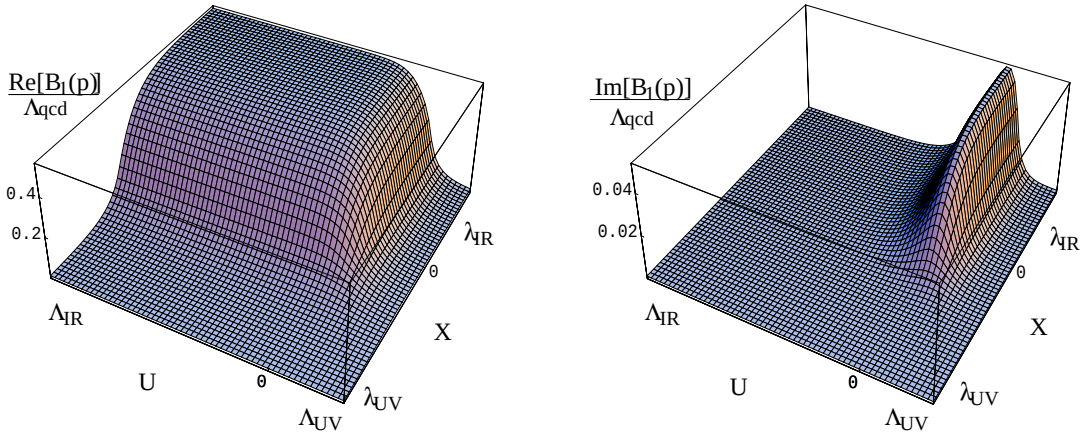

Figure 11 : Momentum dependence of Dirac mass function $B_1(p)/\Lambda_{\rm qcd}$ at $\mu/\Lambda_{\rm qcd} = 0.30$.

We show the resultant values of $-\langle\bar{\psi}\psi\rangle^{1/3}_{1GeV}/\Lambda_{\rm qcd}$ and $|\bar{V}_{\rm sol}|^{1/4}/\Lambda_{\rm qcd}\cdot{\rm sgn}[\bar{\rm V}_{\rm sol}]$ in Figs. 12 and 13, respectively. When one sees Fig. 12 only, one might say that the phase transition occurs around $\mu/\Lambda_{\rm qcd} = 0.40$ (In Ref [24] the chiral phase transition point was determined by the point where their iteration converged to the trivial solution.). However, Fig. 13 shows that the value of $\bar{V}_{\rm sol}$ is positive for $0.36 < \mu/\Lambda_{\rm qcd} < 0.40$ although it is negative for $\mu/\Lambda_{\rm qcd} < 0.36$. In other words, the value of the effective potential of the χSB vacuum for $0.36 < \mu/\Lambda_{\rm qcd} < 0.40$ is larger than that of the symmetric vacuum. This implies that the χSB vacuum for $0.36 < \mu/\Lambda_{\rm qcd} < 0.40$ is the false vacuum, and that the nontrivial solutions there correspond to metastable states. Existence of the metastable states was pointed in Ref. [29] by assuming the momentum dependence of the mass function, and was also shown in Ref. [25] by fully solving the SDE. The value of the critical chemical potential $\mu_c/\Lambda_{\rm qcd} \simeq 0.36$ in the present analysis is smaller than that obtained in Ref. [25] where the screening mass of the gluon was not included and a slightly different form of the running coupling was used.

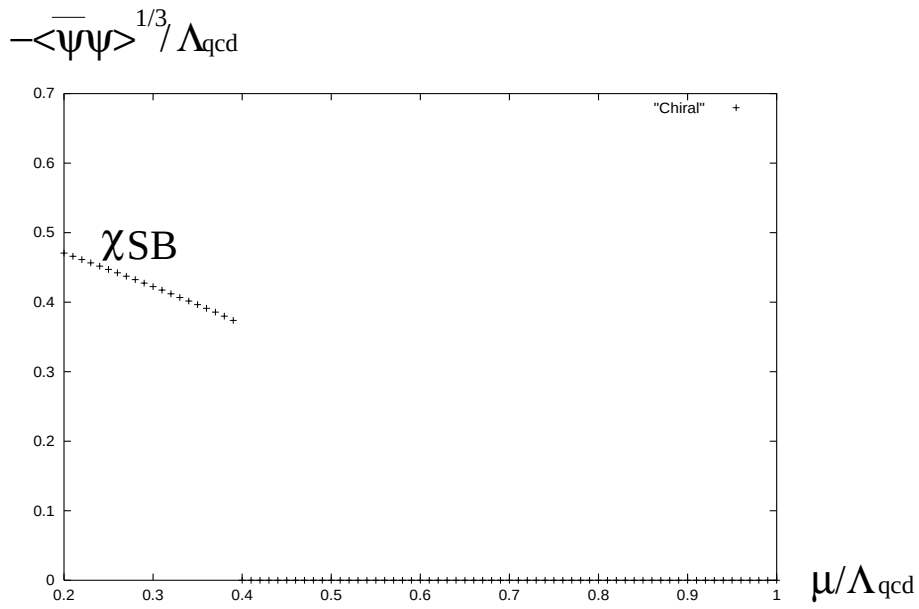

Figure 12: Chemical potential dependence of $\langle\bar{\psi}\psi\rangle_{1GeV}/\Lambda_{\rm qcd}^3$ for $0.2 \leq \mu/\Lambda_{\rm qcd} \leq 1.0$.

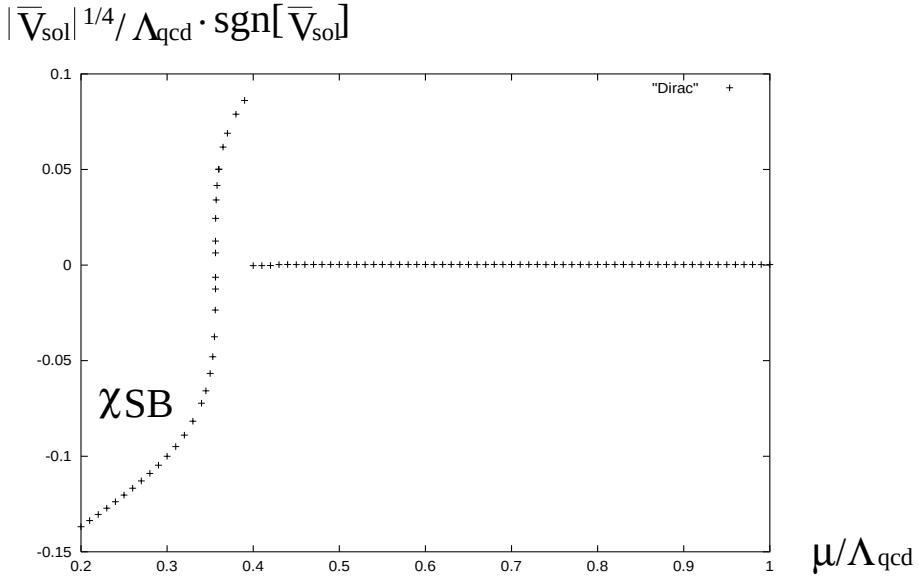

Figure 13: Chemical potential dependence of $|\bar{V}_{\rm sol}|^{1/4}/\Lambda_{\rm qcd} \cdot {\rm sgn}[\bar{\rm V}_{\rm sol}]$ for $0.2 \leq \mu/\Lambda_{\rm qcd} \leq 1.0$.

4.4 Phase transition from hadronic phase to superconducting phase

In this subsection we compare the values of the effective potential for the CSB solution with that for the χSB solution to determin the true vacuum. We combine the effective potential for the CSB solution in Fig. 8 with that for the χSB solution in Fig. 13, and show them in Fig. 14. Figure 14 shows that, although the CSB vacuum is more stable than the trivial vacuum, the χSB vacuum is most stable among these vacua in the low density region. So the true vacuum in the low density region is the χSB vacuum. This is natural because the strength of the attractive force between two quarks in $\bar{3}$ channel is weaker than that between quark and antiquark in the singlet channel. We find that the chiral phase transition and the color superconducting phase transition occur simultaneously at $\mu_c/\Lambda_{\rm qcd} = 0.344.$ and that the phase transition is of first order. We note that this phase transition occurs at lower density than the chiral phase transition in the absence of the color superconductivity.

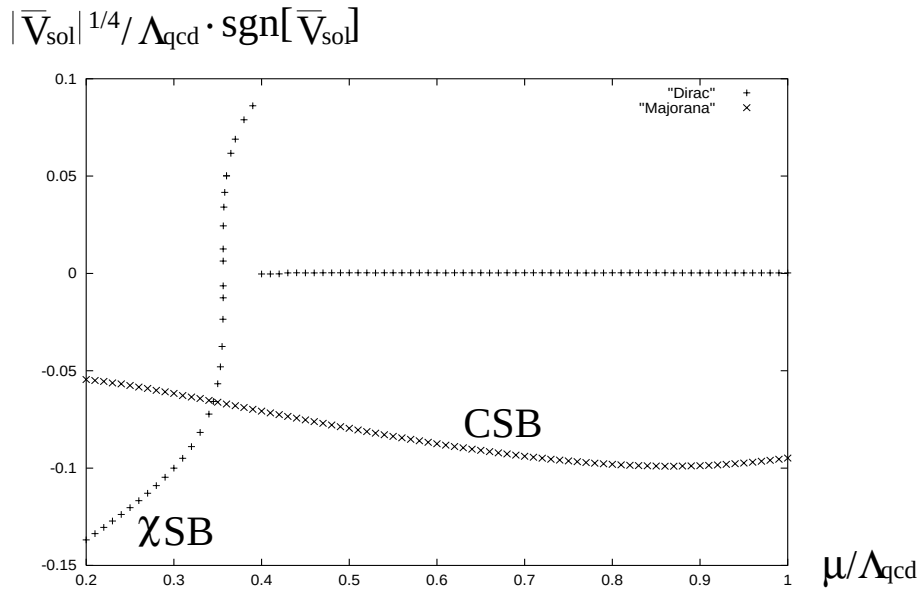

Figure 14: Values of $|\bar{V}_{\rm sol}|^{1/4}/\Lambda_{\rm qcd} \cdot {\rm sgn}[\bar{V}_{\rm sol}]$ $(0.2 \leq \mu/\Lambda_{\rm qcd} \leq 1.0)$. "$\chi$SB" implies that the inputs $B \neq 0$ and $\Delta = 0$ are used, while "CSB" implies that we use $B = 0$ and $\Delta \neq 0$ as initial trial functions.

For comparing the diquark condensate with the chiral condensate, we show them

together in Fig. 15. Note that these are scaled to 1 GeV by the renormalization group formulas shown in Eqs. (2.49) and (2.51). This figure shows that the diquark condensate for all μ is of the same order as the chiral condensate in the low density region. The resultant values of these condensates at the critical chemical potential are $\langle\bar{\psi}\psi\rangle_{1\mathrm{GeV}} = -(241\,\mathrm{MeV})^3$ and $\langle\psi\psi\rangle_{1\mathrm{GeV}} = -(166\,\mathrm{MeV})^3$.

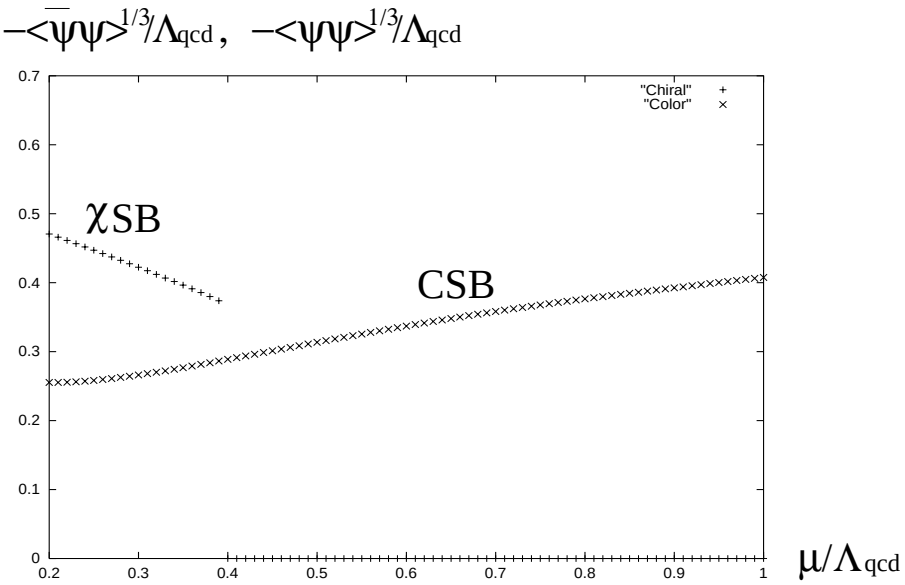

Figure 15: Values of $-\langle\bar{\psi}\psi\rangle^{1/3}_{1GeV}/\Lambda_{\mathrm{qcd}}$ and $-\langle\psi\psi\rangle^{1/3}_{1GeV}/\Lambda_{\mathrm{qcd}}$ ($0.2 \leq \mu/\Lambda_{\mathrm{qcd}} \leq 1.0$). Here "$\chi$SB" implies the chiral condensate $\langle\bar{\psi}\psi\rangle$ and "CSB" implies the diquark condensate $\langle\psi\psi\rangle$.

t_f	Λ_{qcd}[MeV]	μ_c[MeV]	$-\langle\bar{\psi}\psi\rangle^{1/3}_{1GeV}$[MeV]	$-\langle\psi\psi\rangle^{1/3}_{1GeV}$[MeV]
0.3	568	210	223	169
0.4	579	207	231	168
0.5	604	208	241	166
0.6	647	214	254	167
0.7	712	223	269	168

Table 1: Dependence of the critical chemical potential μ_c on the infrared cutoff parameter t_f. Λ_{qcd} is the value determined from $f_\pi = 88$ MeV through Eq. (4.1). The values of the chiral condensate $\langle\bar{\psi}\psi\rangle$ and the diquark condensate $\langle\psi\psi\rangle$ shown together are at the critical chemical potential μ_c.

Finally, let us check the t_f dependence of the critical chemical potential. We give the values of the critical chemical potential μ_c for t_f=0.3$\sim$0.7 in Table 1, together with the values of the chiral condensate and the diquark condensate at μ_c. This table shows that the value of μ_c is almost independent of the value of t_f. Although the value of $\langle\bar{\psi}\psi\rangle$ slightly depends on that of t_f, $\langle\psi\psi\rangle$ is quite stable against the change of t_f.

5 Summary and Discussion

We studied the phase structure in two-flavor dense QCD by solving the Schwinger-Dyson equations for the Dirac and the Majorana masses of the quark propagator with the improved ladder approximation in the Landau gauge.

The values of the chiral condensate (quark-antiquark condensate) and the diquark condensate were calculated by the standard formulas. We identified the condensates, which were calculated with the cutoffs Λ, with those renormalized at scale Λ in QCD, and then scaled them to the condensates at 1 GeV using the leading renormalization group formulas. The resultant value of the diquark condensate is on the order of $-(200\,\mathrm{MeV})^3$, which is comparable to the chiral condensate for $\mu = 0$.

The true vacuum was determined by comparing the values of the effective potential at the solution. We found that there exists color symmetry breaking (CSB) solution for all the values of the chemical potential we studied, $0.2 \leq \mu/\Lambda_{\mathrm{qcd}} \leq 1$, and that the CSB vacuum is more stable than the trivial vacuum in all region. Comparing the value of the effective potential for the CSB vacuum with that for the chiral symmetry breaking (χSB) vacuum, we showed that the χSB vacuum is more stable than the CSB vacuum in the low density region. We found that the phase transition from the χSB vacuum to the CSB vacuum is of first order. The critical chemical potential was determined as $\mu_c = 207$-$223\,\mathrm{MeV}$.

Finally, we make several comments. In an analysis by the four-Fermi model [11], it seems to be shown that there is a mixed phase, where both the chiral condensate and the diquark condensate exist, in the small region of the chemical potential. In our analysis, we tried to find the solution corresponding to the mixed phase. However, we could not find such a solution in the present iteration method although we used several initial trial

functions.

In the present analysis we included the Debye mass of the gluon using the hard dense loop approximation [6], with assuming the smooth extraporation from the high density region. As we can see easily from the expression in Eq. (2.33), the form of the magnetic mode explicitly breaks the Lorentz invariance, so that we cannot apply the same form near $\mu = 0$. It may be interesting to compare the present results with those obtained by using the gluon propagator of the magnetic mode for $\mu = 0$ in the low density region. This will be done elsewhere.

Acknowledgment

This work is supported in part by Grant-in-Aid for Scientific Research (A)#12740144 (M.H.)

A Quark Propagator and Schwinger-Dyson Equation

The explicit forms of the Nambu-Gorkov components of the full quark propagator in Eq. (2.31) are given by

$$
\begin{aligned}
S_{F11}(p)_{ij}^{ab} &= S_{F22}(p)_{ij}^{ab}|[\mu \to -\mu; B(p) \to B(-p); \Delta^{\pm}(p) \to -\Delta^{\mp}(p)] \\
&= iR_{+}(p)^{-1}{}_{ij}^{ab} \\
&= \frac{i}{F(p, B_1, \Delta)} \\
&\quad \Big[\Big\{\Big((p_0 - \bar{p} + \mu)[(p_0 - \mu)^2 - \bar{p}^2 - \{B_1(-p)\}^2] - (p_0 - \bar{p} - \mu)|\Delta^{-}(p)|^2\Big)\gamma_0 \\
&\qquad -B_1(-p)\Delta^{-}(p)\Delta^{+}(p) + B_1(p)[(p_0 - \mu)^2 - \bar{p}^2 - \{B_1(-p)\}^2]\Big\}\Lambda_p^{+} \\
&\quad +\Big\{\Big((p_0 + \bar{p} + \mu)[(p_0 - \mu)^2 - \bar{p}^2 - \{B_1(-p)\}^2] - (p_0 + \bar{p} - \mu)|\Delta^{+}(p)|^2\Big)\gamma_0 \\
&\qquad -B_1(-p)\Delta^{+}(p)\Delta^{-}(p) + B_1(p)[(p_0 - \mu)^2 - \bar{p}^2 - \{B_1(-p)\}^2]\Big\}\Lambda_p^{-}\Big]\delta_{ij}\tilde{\delta}^{ab} \\
&\quad +\frac{i}{(p_0 + \mu)^2 - \bar{p}^2 - \{B_3(p)\}^2}\Big[\Big\{(p_0 - \bar{p} + \mu)\gamma_0 + B_3(p)\Big\}\Lambda_p^{+}
\end{aligned}
$$

$$+\Big\{(p_0+\bar{p}+\mu)\gamma_0+B_3(p)\Big\}\Lambda_p^-\Big]\delta_{ij}\delta^{a3}\delta^{b3}\ , \tag{A.1}$$

$$\begin{aligned}
S_{F12}(p)_{ij}^{ab} &= S_{F21}(p)_{ij}^{ab}|[\mu\to-\mu;B(p)\to B(-p);\Delta^{\pm}(p)\to-\Delta^{\mp}(p)] \\
&= -i\{(p_0+\mu)\gamma^0-\vec{\gamma}\cdot\vec{p}-m(p)\}^{-1}\Delta(p)R_-(p)^{-1}{}_{ij}^{ab} \\
&= \frac{-i}{F(p,B_1,\Delta)}\Big[\Big\{\Big((p_0-\bar{p}+\mu)\Delta^+(p)B_1(-p)-(p_0-\bar{p}-\mu)\Delta^-(p)B_1(p)\Big)\gamma_0 \\
&\quad+\Big(|B_1(p)|^2\Delta^+(p)-[(p_0)^2-(\bar{p}+\mu)^2-|\Delta^+(p)|^2]\Delta^-(p)\Big)\Big\}\Lambda_p^+ \\
&\quad+\Big\{\Big((p_0+\bar{p}+\mu)\Delta^-(p)B_1(-p)-(p_0+\bar{p}-\mu)\Delta^+(p)B_1(p)\Big)\gamma_0 \\
&\quad+\Big(|B_1(p)|^2\Delta^-(p)-[(p_0)^2-(\bar{p}-\mu)^2-|\Delta^-(p)|^2]\Delta^+(p)\Big)\Big\}\Lambda_p^-\Big]\gamma_5\epsilon_{ij}\epsilon^{ab3}\ ,
\end{aligned} \tag{A.2}$$

where

$$\begin{aligned}
F(p,B_1,\Delta) &= [(p_0+\mu)^2-\bar{p}^2-\{B_1(p)\}^2][(p_0-\mu)^2-\bar{p}^2-\{B_1(-p)\}^2] \\
&\quad-[(p_0)^2-(\bar{p}-\mu)^2]|\Delta^+(p)|^2-[(p_0)^2-(\bar{p}+\mu)^2]|\Delta^-(p)|^2 \\
&\quad+|\Delta^+(p)|^2|\Delta^-(p)|^2+2B_1(p)B_1(-p)\Delta^+(p)\Delta^-(p)\ .
\end{aligned} \tag{A.3}$$

Substituting the expression of S_{F11} in Eq. (A.1) into the SDE's for B_1 and B_3 in Eqs. (3.6) and (3.7), we obtain

$$\begin{aligned}
B_1(p) &= -2\pi\int_{-\infty}^{\infty}\frac{dq_4}{(2\pi)^4}\int d\bar{q}\bar{q}^2\alpha_s \\
&\quad\times K_0(q_4,p_4,\bar{q},\bar{p})\Big[\frac{5}{6}\frac{F_+(q,B_1,\Delta)}{F(q,B_1,\Delta)}+\frac{1}{2}\frac{B_3(q)}{(iq_4+\mu)^2-\bar{q}^2-\{B_3(q)\}^2}\Big]\quad,
\end{aligned} \tag{A.4}$$

$$\begin{aligned}
B_3(p) &= -2\pi\int_{-\infty}^{\infty}\frac{dq_4}{(2\pi)^4}\int d\bar{q}\bar{q}^2\alpha_s \\
&\quad\times K_0(q_4,p_4,\bar{q},\bar{p})\Big[\frac{F_+(q,B_1,\Delta)}{F(q,B_1,\Delta)}+\frac{1}{3}\frac{B_3(q)}{(iq_4+\mu)^2-\bar{q}^2-\{B_3(q)\}^2}\Big]\quad,
\end{aligned} \tag{A.5}$$

where

$$F_+(q,B_1,\Delta) = B_1(q)[(iq_4-\mu)^2-\bar{q}^2-\{B_1(-q)\}^2]-B_1(-q)\Delta^+(q)\Delta^-(q)\quad,$$

(A.6)

$$F_-(q,B_1,\Delta) = B_1(-q)[(iq_4+\mu)^2-\bar{q}^2-\{B_1(q)\}^2]-B_1(q)\Delta^+(q)\Delta^-(q) \quad , \tag{A.7}$$

with $q_4=-iq_0$ and $p_4=-ip_0$. The integration kernel K_0 is given by

$$\begin{aligned} K_0(q_4,p_4,\bar{q},\bar{p}) &= -i\int d\Omega D_{F\mu\nu}(q-p)\mathrm{tr}(\gamma^\mu\Lambda_q^\pm\gamma^\nu) \\ &= 4\cdot\frac{2\pi}{3\bar{q}\bar{p}}\log\frac{|\bar{q}+\bar{p}|^3+\omega_l^3}{|\bar{q}-\bar{p}|^3+\omega_l^3}+2\cdot(1+d)\frac{\pi}{\bar{q}\bar{p}}\log\frac{|\bar{q}+\bar{p}|^2+\omega^2+2M_D^2}{|\bar{q}-\bar{p}|^2+\omega^2+2M_D^2} \quad , \end{aligned} \tag{A.8}$$

where

$$\begin{aligned} \omega_l^3 &= \frac{\pi}{2}M_D^2\omega \ , \qquad \omega = |q_4-p_4| \ , \\ \bar{\omega}_l^3 &= \frac{\pi}{2}M_D^2\bar{\omega} \ , \qquad \bar{\omega} = |q_4+p_4| \ . \end{aligned} \tag{A.9}$$

When we take $\Delta^-=\Delta^+=0$, we have

$$\frac{F_\pm(q,B_1,\Delta=0)}{F(q,B_1,\Delta=0)} = \frac{B_1(q)}{(iq_4\pm\mu)^2-\bar{q}^2-\{B_1(q)\}^2} \ . \tag{A.10}$$

If we further take $B_1=B_3$, two equations in Eqs. (A.4) and (A.5) agree with each other. This implies that $B_1=B_3$ is actually a solution of the SDE's for $\Delta^\pm=0$.

Next, substituting Eq. (A.2) into the SDE's for Δ^- and Δ^+ in Eqs. (3.8) and (3.9), we obtain

$$\begin{aligned} \Delta^-(p) &= 2\pi\int_{-\infty}^{\infty}\frac{dq_4}{(2\pi)^4}\int d\bar{q}\bar{q}^2\alpha_s \\ &\quad\times\left[K_1(q_4,p_4,\bar{q},\bar{p})\cdot\frac{2}{3}\cdot\frac{G_+(q,B_1,\Delta)}{F(q,B_1,\Delta)}+K_2(q_4,p_4,\bar{q},\bar{p})\cdot\frac{2}{3}\cdot\frac{G_-(q,B_1,\Delta)}{F(q,B_1,\Delta)}\right] , \end{aligned} \tag{A.11}$$

$$\begin{aligned} \Delta^+(p) &= 2\pi\int_{-\infty}^{\infty}\frac{dq_4}{(2\pi)^4}\int d\bar{q}\bar{q}^2\alpha_s \\ &\quad\times\left[K_1(q_4,p_4,\bar{q},\bar{p})\cdot\frac{2}{3}\cdot\frac{G_-(q,B_1,\Delta)}{F(q,B_1,\Delta)}+K_2(q_4,p_4,\bar{q},\bar{p})\cdot\frac{2}{3}\cdot\frac{G_+(q,B_1,\Delta)}{F(q,B_1,\Delta)}\right] , \end{aligned} \tag{A.12}$$

where

$$G_+(q,B_1,\Delta) = B_1(q)B_1(-q)\Delta^+(q)+[(q_4)^2+(\bar{q}+\mu)^2+|\Delta^+(q)|^2]\Delta^-(q) \ ,$$

(A.13)

$$G_-(q,B_1,\Delta) \;=\; B_1(q)B_1(-q)\Delta^-(q) + [(q_4)^2 + (\bar{q}-\mu)^2 + |\Delta^-(q)|^2]\Delta^+(q)\ .$$

(A.14)

The integration kernels K_1 and K_2 are given by

$$\begin{aligned}
K_1(q_4,p_4,\bar{q},\bar{p}) &= -i\int d\Omega D_{F\mu\nu}(q-p)\mathrm{tr}(\Lambda_p^{\pm}\gamma^\mu\Lambda_q^{\mp}\gamma^\nu) \\
&= -\pi\frac{(\bar{q}^2-\bar{p}^2)^2+\omega_l^4}{\sqrt{3}\omega_l^2\bar{q}^2\bar{p}^2}\arctan\Big(\frac{\sqrt{3}\omega_l\min(\bar{q},\bar{p})}{\omega_l^2+|\bar{q}^2-\bar{p}^2|-\omega_l\max(\bar{q},\bar{p})}\Big) \\
&\quad -\pi\frac{(\bar{q}^2-\bar{p}^2)^2-\omega_l^4}{3\omega_l^2\bar{q}^2\bar{p}^2}\ln\frac{\omega_l+|\bar{q}+\bar{p}|}{\omega_l+|\bar{q}-\bar{p}|} + \pi\frac{(\bar{q}^2-\bar{p}^2)^2-\omega_l^4}{6\omega_l^2\bar{q}^2\bar{p}^2}\ln\frac{\omega_l^2+|\bar{q}+\bar{p}|^2-\omega_l|\bar{q}+\bar{p}|}{\omega_l^2+|\bar{q}-\bar{p}|^2-\omega_l|\bar{q}-\bar{p}|} \\
&\quad +\pi\frac{4}{3\bar{q}\bar{p}}\ln\frac{\omega_l^3+|\bar{q}+\bar{p}|^3}{\omega_l^3+|\bar{q}-\bar{p}|^3} + \frac{\pi}{2\bar{q}^2\bar{p}^2}\Big[\frac{(\bar{q}^2-\bar{p}^2)^2}{2M_D^2+\omega^2}\ln\frac{(\bar{q}+\bar{p})^2}{(\bar{q}-\bar{p})^2} \\
&\qquad +\frac{\{(\bar{q}+\bar{p})^2+2M_D^2+\omega^2\}\{(2M_D^2+\omega^2)^2+(\bar{q}-\bar{p})^2\omega^2\}}{2M_D^2(2M_D^2+\omega^2)}\ln\frac{(\bar{q}+\bar{p})^2+2M_D^2+\omega^2}{(\bar{q}-\bar{p})^2+2M_D^2+\omega^2} \\
&\qquad -\frac{\{(\bar{q}+\bar{p})^2+\omega^2\}\{(\bar{q}-\bar{p})^2+\omega^2\}}{2M_D^2}\ln\frac{(\bar{q}+\bar{p})^2+\omega^2}{(\bar{q}-\bar{p})^2+\omega^2}\Big] \\
&\quad +\pi d\Big[\frac{2}{\bar{q}\bar{p}} - \frac{(\bar{q}-\bar{p})^2+\omega^2}{2\bar{q}^2\bar{p}^2}\ln\frac{(\bar{q}+\bar{p})^2+\omega^2}{(\bar{q}-\bar{p})^2+\omega^2}\Big]\ ,
\end{aligned}$$

(A.15)

$$\begin{aligned}
K_2(q_4,p_4,\bar{q},\bar{p}) &= -i\int d\Omega D_{F\mu\nu}(q-p)\mathrm{tr}(\Lambda_p^{\pm}\gamma^\mu\Lambda_q^{\pm}\gamma^\nu) \\
&= \pi\frac{(\bar{q}^2-\bar{p}^2)^2+\omega_l^4}{\sqrt{3}\omega_l^2\bar{q}^2\bar{p}^2}\arctan\Big(\frac{\sqrt{3}\omega_l\min(\bar{q},\bar{p})}{\omega_l^2+|\bar{q}^2-\bar{p}^2|-\omega_l\max(\bar{q},\bar{p})}\Big) \\
&\quad +\pi\frac{(\bar{q}^2-\bar{p}^2)^2-\omega_l^4}{3\omega_l^2\bar{q}^2\bar{p}^2}\ln\frac{\omega_l+|\bar{q}+\bar{p}|}{\omega_l+|\bar{q}-\bar{p}|} - \pi\frac{(\bar{q}^2-\bar{p}^2)^2-\omega_l^4}{6\omega_l^2\bar{q}^2\bar{p}^2}\ln\frac{\omega_l^2+|\bar{q}+\bar{p}|^2-\omega_l|\bar{q}+\bar{p}|}{\omega_l^2+|\bar{q}-\bar{p}|^2-\omega_l|\bar{q}-\bar{p}|} \\
&\quad +\pi\frac{4}{3\bar{q}\bar{p}}\ln\frac{\omega_l^3+|\bar{q}+\bar{p}|^3}{\omega_l^3+|\bar{q}-\bar{p}|^3} - \frac{\pi}{2\bar{q}^2\bar{p}^2}\Big[\frac{(\bar{q}^2-\bar{p}^2)^2}{2M_D^2+\omega^2}\ln\frac{(\bar{q}+\bar{p})^2}{(\bar{q}-\bar{p})^2} \\
&\qquad +\frac{\{(\bar{q}-\bar{p})^2+2M_D^2+\omega^2\}\{(2M_D^2+\omega^2)^2+(\bar{q}+\bar{p})^2\omega^2\}}{2M_D^2(2M_D^2+\omega^2)}\ln\frac{(\bar{q}+\bar{p})^2+2M_D^2+\omega^2}{(\bar{q}-\bar{p})^2+2M_D^2+\omega^2} \\
&\qquad -\frac{\{(\bar{q}+\bar{p})^2+\omega^2\}\{(\bar{q}-\bar{p})^2+\omega^2\}}{2M_D^2}\ln\frac{(\bar{q}+\bar{p})^2+\omega^2}{(\bar{q}-\bar{p})^2+\omega^2}\Big] \\
&\quad -\pi d\Big[\frac{2}{\bar{q}\bar{p}} - \frac{(\bar{q}+\bar{p})^2+\omega^2}{2\bar{q}^2\bar{p}^2}\ln\frac{(\bar{q}+\bar{p})^2+\omega^2}{(\bar{q}-\bar{p})^2+\omega^2}\Big]\ .
\end{aligned}$$

(A.16)

We note that for $B_1 = 0$ we have

$$\frac{G_\pm(q,B_1=0,\Delta)}{F(q,B_1=0,\Delta)} \;=\; \frac{-\Delta^\mp(q)}{(q_4)^2+(\bar{q}\mp\mu)^2+|\Delta^\mp(q)|^2}\ . \qquad (A.17)$$

Then the SDE's (A.11) and (A.12) agree with the well known forms shown in, e.g., Ref. [6].

B Convenient Formulas

In this appendix we show several convenient formulas to obtain the explicit forms of the Schwinger-Dyson equations and the effective potential shown in Sec. 3 and Appendix A.

As shown in subsection 2.2, we take the Landau gauge in the present analysis, and then two polarization tensors are used in Eq. (2.33). When we take the general covariant gauge as done in Ref. [6], we need three independent polarization tensors defined as

$$O^{(1)}_{\mu\nu} = P^{\perp}_{\mu\nu} + \frac{(u\cdot k)^2}{(u\cdot k)^2 - k^2} P^u_{\mu\nu} \ , \qquad O^{(2)}_{\mu\nu} = -\frac{(u\cdot k)^2}{(u\cdot k)^2 - k^2} P^u_{\mu\nu} \ , \qquad O^{(3)}_{\mu\nu} = \frac{k_\mu k_\nu}{k^2} \ , \tag{B.1}$$

where

$$P^{\perp}_{\mu\nu} = g_{\mu\nu} - \frac{k_\mu k_\nu}{k^2} \ , \qquad P^u_{\mu\nu} = \frac{k_\mu k_\nu}{k^2} - \frac{k_\mu u_\nu + u_\mu k_\nu}{u\cdot k} + \frac{u_\mu u_\nu}{(u\cdot k)^2} k^2 \ . \tag{B.2}$$

The following formulas are convenient to obtain the SDE's:

$$O^{(1)}_{\mu\nu}\mathrm{tr}(\gamma^\mu \Lambda^{\pm}_q \gamma^\nu) = 4 \ , \qquad O^{(i)}_{\mu\nu}\mathrm{tr}(\gamma^\mu \Lambda^{\pm}_q \gamma^\nu) = 2 \ , \qquad (i = 2, 3)$$

$$\begin{aligned}
O^{(1)}_{\mu\nu}\mathrm{tr}(\Lambda^{\pm}_p \gamma^\mu \Lambda^{\pm}_q \gamma^\nu) &= 2(1+t)\frac{\bar{q}^2 + \bar{p}^2 - \bar{q}\bar{p}(1+t)}{\bar{q}^2 + \bar{p}^2 - 2\bar{q}\bar{p}t} \ , \\
O^{(1)}_{\mu\nu}\mathrm{tr}(\Lambda^{\pm}_p \gamma^\mu \Lambda^{\mp}_q \gamma^\nu) &= 2(1-t)\frac{\bar{q}^2 + \bar{p}^2 + \bar{q}\bar{p}(1-t)}{\bar{q}^2 + \bar{p}^2 - 2\bar{q}\bar{p}t} \ , \\
O^{(2)}_{\mu\nu}\mathrm{tr}(\Lambda^{\pm}_p \gamma^\mu \Lambda^{\pm}_q \gamma^\nu) &= 2(1-t)\frac{\bar{q}^2 + \bar{p}^2 + \bar{q}\bar{p}(1-t)}{\bar{q}^2 + \bar{p}^2 - 2\bar{q}\bar{p}t} - (1-t)\frac{(\bar{q}+\bar{p})^2 + (q_4 - p_4)^2}{\bar{q}^2 + \bar{p}^2 - 2\bar{q}\bar{p}t + (q_4 - p_4)^2} \ , \\
O^{(2)}_{\mu\nu}\mathrm{tr}(\Lambda^{\pm}_p \gamma^\mu \Lambda^{\mp}_q \gamma^\nu) &= 2(1+t)\frac{\bar{q}^2 + \bar{p}^2 - \bar{q}\bar{p}(1+t)}{\bar{q}^2 + \bar{p}^2 - 2\bar{q}\bar{p}t} - (1+t)\frac{(\bar{q}-\bar{p})^2 + (q_4 - p_4)^2}{\bar{q}^2 + \bar{p}^2 - 2\bar{q}\bar{p}t + (q_4 - p_4)^2} \ , \\
O^{(3)}_{\mu\nu}\mathrm{tr}(\Lambda^{\pm}_p \gamma^\mu \Lambda^{\pm}_q \gamma^\nu) &= (1-t)\frac{(\bar{q}+\bar{p})^2 + (q_4 - p_4)^2}{\bar{q}^2 + \bar{p}^2 - 2\bar{q}\bar{p}t + (q_4 - p_4)^2} \ , \\
O^{(3)}_{\mu\nu}\mathrm{tr}(\Lambda^{\pm}_p \gamma^\mu \Lambda^{\mp}_q \gamma^\nu) &= (1+t)\frac{(\bar{q}-\bar{p})^2 + (q_4 - p_4)^2}{\bar{q}^2 + \bar{p}^2 - 2\bar{q}\bar{p}t + (q_4 - p_4)^2} \ ,
\end{aligned} \tag{B.3}$$

where $t = \vec{p}\cdot\vec{q}/|p||q|$. Angle integrations in the SDE's are performed by using the following formulas[6]:

$$\int \frac{d\Omega |\vec{q} - \vec{p}|}{|\vec{q} - \vec{p}|^3 + \omega_l^3} = \frac{2\pi}{3\bar{q}\bar{p}} \log \frac{|\bar{q} + \bar{p}|^3 + \omega_l^3}{|\bar{q} - \bar{p}|^3 + \omega_l^3} \ ,$$

$$\int \frac{d\Omega}{|\vec{q} - \vec{p}|^2 + \omega^2 + 2M_D^2} = \frac{\pi}{\bar{q}\bar{p}} \log \frac{|\bar{q} + \bar{p}|^2 + \omega^2 + 2M_D^2}{|\bar{q} - \bar{p}|^2 + \omega^2 + 2M_D^2} \ ,$$

$$
\begin{aligned}
&\int \frac{d\Omega|\vec{q}-\vec{p}|}{|\vec{q}-\vec{p}|^3+\omega_l^3} O^{(1)}_{\mu\nu}\mathrm{tr}(\Lambda^{\pm}_p\gamma^\mu\Lambda^{\pm}_q\gamma^\nu) \\
&\quad = \pi\Big[-\frac{2}{\bar{q}\bar{p}} - \frac{(\bar{q}^2-\bar{p}^2)^2+\omega_l^4}{\sqrt{3}\omega_l^2\bar{q}^2\bar{p}^2}\arctan\Big(\frac{\sqrt{3}\omega_l\min(\bar{q},\bar{p})}{\omega_l^2+|\bar{q}^2-\bar{p}^2|-\omega_l\max(\bar{q},\bar{p})}\Big) \\
&\qquad + \frac{(\bar{q}^2-\bar{p}^2)^2-\omega_l^4}{3\omega_l^2\bar{q}^2\bar{p}^2}\ln\frac{\omega_l+|\bar{q}+\bar{p}|}{\omega_l+|\bar{q}-\bar{p}|} - \frac{(\bar{q}^2-\bar{p}^2)^2-\omega_l^4}{6\omega_l^2\bar{q}^2\bar{p}^2}\ln\frac{\omega_l^2+|\bar{q}+\bar{p}|^2-\omega_l|\bar{q}+\bar{p}|}{\omega_l^2+|\bar{q}-\bar{p}|^2-\omega_l|\bar{q}-\bar{p}|} \\
&\qquad + \frac{4}{3\bar{q}\bar{p}}\ln\frac{\omega_l^3+|\bar{q}+\bar{p}|^3}{\omega_l^3+|\bar{q}-\bar{p}|^3}\Big]\,,
\end{aligned}
$$

$$
\begin{aligned}
&\int \frac{d\Omega|\vec{q}-\vec{p}|}{|\vec{q}-\vec{p}|^3+\omega_l^3} O^{(1)}_{\mu\nu}\mathrm{tr}(\Lambda^{\pm}_p\gamma^\mu\Lambda^{\mp}_q\gamma^\nu) \\
&\quad = \pi\Big[\frac{2}{\bar{q}\bar{p}} - \frac{(\bar{q}^2-\bar{p}^2)^2+\omega_l^4}{\sqrt{3}\omega_l^2\bar{q}^2\bar{p}^2}\arctan\Big(\frac{\sqrt{3}\omega_l\min(\bar{q},\bar{p})}{\omega_l^2+|\bar{q}^2-\bar{p}^2|-\omega_l\max(\bar{q},\bar{p})}\Big) \\
&\qquad - \frac{(\bar{q}^2-\bar{p}^2)^2-\omega_l^4}{3\omega_l^2\bar{q}^2\bar{p}^2}\ln\frac{\omega_l+|\bar{q}+\bar{p}|}{\omega_l+|\bar{q}-\bar{p}|} + \frac{(\bar{q}^2-\bar{p}^2)^2-\omega_l^4}{6\omega_l^2\bar{q}^2\bar{p}^2}\ln\frac{\omega_l^2+|\bar{q}+\bar{p}|^2-\omega_l|\bar{q}+\bar{p}|}{\omega_l^2+|\bar{q}-\bar{p}|^2-\omega_l|\bar{q}-\bar{p}|} \\
&\qquad + \frac{4}{3\bar{q}\bar{p}}\ln\frac{\omega_l^3+|\bar{q}+\bar{p}|^3}{\omega_l^3+|\bar{q}-\bar{p}|^3}\Big]\,,
\end{aligned}
$$

$$
\begin{aligned}
&\int \frac{d\Omega}{|\vec{q}-\vec{p}|^2+\omega^2+2M_D^2} O^{(2)}_{\mu\nu}\mathrm{tr}(\Lambda^{\pm}_p\gamma^\mu\Lambda^{\pm}_q\gamma^\nu) \\
&\quad = \frac{2\pi}{\bar{q}\bar{p}} + \frac{\pi}{2\bar{q}^2\bar{p}^2}\Big[-\frac{(\bar{q}^2-\bar{p}^2)^2}{2M_D^2+\omega^2}\ln\frac{(\bar{q}+\bar{p})^2}{(\bar{q}-\bar{p})^2} \\
&\qquad - \frac{\{(\bar{q}-\bar{p})^2+2M_D^2+\omega^2\}\{(2M_D^2+\omega^2)^2+(\bar{q}+\bar{p})^2\omega^2\}}{2M_D^2(2M_D^2+\omega^2)}\ln\frac{(\bar{q}+\bar{p})^2+2M_D^2+\omega^2}{(\bar{q}-\bar{p})^2+2M_D^2+\omega^2} \\
&\qquad + \frac{\{(\bar{q}+\bar{p})^2+\omega^2\}\{(\bar{q}-\bar{p})^2+\omega^2\}}{2M_D^2}\ln\frac{(\bar{q}+\bar{p})^2+\omega^2}{(\bar{q}-\bar{p})^2+\omega^2}\Big]\,,
\end{aligned}
$$

$$
\begin{aligned}
&\int \frac{d\Omega}{|\vec{q}-\vec{p}|^2+\omega^2+2M_D^2} O^{(2)}_{\mu\nu}\mathrm{tr}(\Lambda^{\pm}_p\gamma^\mu\Lambda^{\mp}_q\gamma^\nu) \\
&\quad = -\frac{2\pi}{\bar{q}\bar{p}} + \frac{\pi}{2\bar{q}^2\bar{p}^2}\Big[\frac{(\bar{q}^2-\bar{p}^2)^2}{2M_D^2+\omega^2}\ln\frac{(\bar{q}+\bar{p})^2}{(\bar{q}-\bar{p})^2} \\
&\qquad + \frac{\{(\bar{q}+\bar{p})^2+2M_D^2+\omega^2\}\{(2M_D^2+\omega^2)^2+(\bar{q}-\bar{p})^2\omega^2\}}{2M_D^2(2M_D^2+\omega^2)}\ln\frac{(\bar{q}+\bar{p})^2+2M_D^2+\omega^2}{(\bar{q}-\bar{p})^2+2M_D^2+\omega^2} \\
&\qquad - \frac{\{(\bar{q}+\bar{p})^2+\omega^2\}\{(\bar{q}-\bar{p})^2+\omega^2\}}{2M_D^2}\ln\frac{(\bar{q}+\bar{p})^2+\omega^2}{(\bar{q}-\bar{p})^2+\omega^2}\Big]\,,
\end{aligned}
$$

$$
\begin{aligned}
\int \frac{d\Omega}{|\vec{q}-\vec{p}|^2+\omega^2} O^{(3)}_{\mu\nu}\mathrm{tr}(\Lambda^{\pm}_p\gamma^\mu\Lambda^{\pm}_q\gamma^\nu) &= \pi\Big[-\frac{2}{\bar{q}\bar{p}} + \frac{(\bar{q}-\bar{p})^2+\omega^2}{2\bar{q}^2\bar{p}^2}\ln\frac{(\bar{q}+\bar{p})^2+\omega^2}{(\bar{q}-\bar{p})^2+\omega^2}\Big], \\
\int \frac{d\Omega}{|\vec{q}-\vec{p}|^2+\omega^2} O^{(3)}_{\mu\nu}\mathrm{tr}(\Lambda^{\pm}_p\gamma^\mu\Lambda^{\mp}_q\gamma^\nu) &= \pi\Big[\frac{2}{\bar{q}\bar{p}} - \frac{(\bar{q}-\bar{p})^2+\omega^2}{2\bar{q}^2\bar{p}^2}\ln\frac{(\bar{q}+\bar{p})^2+\omega^2}{(\bar{q}-\bar{p})^2+\omega^2}\Big]\,.
\end{aligned}
\tag{B.4}
$$

Here we list the products of the color matrices in the SDE. The completeness relation leads to

$$\sum_{A=1}^{8}(T^A)_{a'a}(T^A)_{b'b} = \frac{1}{2}\delta_{a'b}\delta_{ab'} - \frac{1}{6}\delta_{aa'}\delta_{bb'} \ . \tag{B.5}$$

By using the above formula the products of the color matrices in the SDE's (3.6) and (3.7) are written as

$$\begin{aligned}\sum_{A=1}^{8}(T^A)_{aa'}\tilde{\delta}^{a'b'}(T^A)_{b'b} &= \frac{5}{6}\tilde{\delta}_{ab} + \delta_{a3}\delta_{b3}, \\ \sum_{A=1}^{8}(T^A)_{aa'}\delta_{a'3}\delta_{b'3}(T^A)_{b'b} &= \frac{1}{2}\tilde{\delta}_{ab} + \frac{1}{3}\delta_{a3}\delta_{b3}.\end{aligned} \tag{B.6}$$

The product in the SDE's (3.8) and (3.9) is written as

$$\sum_{A=1}^{8}(T^A)_{aa'}\epsilon^{a'b'3}(T^A)_{bb'} = -\frac{2}{3}\epsilon^{ab3}. \tag{B.7}$$

To obtain the effective potential we need to take the trace and the determinant over the color, flavor, spinor and Nambu-Gorkov indices. The determinant in the first term in Eq. (3.1) is given by

$$\mathrm{Det}\{iS_F(p)^{-1}\} = \{F(p,B_1,\Delta)\}^8\{F(p,B_3,0)\}^4 \quad . \tag{B.8}$$

The trace in the second term becomes

$$\begin{aligned}\mathrm{Tr}\{S_F^{(0)}(p)^{-1}S_F(p)\} = 8\Big[&\frac{2}{F(p,B_1,\Delta)}\Big\{2(p_+^2-\bar{p}^2)(p_-^2-\bar{p}^2) \\ &-(p_+^2-\bar{p}^2)\{B_1(-p)\}^2-(p_-^2-\bar{p}^2)\{B_1(p)\}^2 \\ &-\Big((p_0)^2-(\bar{p}+\mu)^2\Big)|\Delta^-|^2-\Big((p_0)^2-(\bar{p}-\mu)^2\Big)|\Delta^+|^2\Big\} \\ &+\frac{(p_0+\mu)^2-\bar{p}^2}{(p_0+\mu)^2-\bar{p}^2-\{B_3(p)\}^2}+\frac{(p_0-\mu)^2-\bar{p}^2}{(p_0-\mu)^2-\bar{p}^2-\{B_3(-p)\}^2}\Big] \quad .\end{aligned} \tag{B.9}$$

References

[1] G. E. Brown and M. Rho, hep-ph/0103102; Phys. Rept. **269**, 333 (1996) [hep-ph/9504250];
F. Wilczek, hep-ph/0003183.
S. P. Klevansky, hep-ph/9810399;
R. D. Pisarski, hep-ph/9503330;
T. Hatsuda and T. Kunihiro, Phys. Rept. **247**, 221 (1994) [hep-ph/9401310].

[2] B. C. Barrois, Nucl. Phys. B **129**, 390 (1977).

[3] D. Bailin and A. Love, Phys. Rept. **107**, 325 (1984).

[4] M. Alford, K. Rajagopal and F. Wilczek, Phys. Lett. B **422**, 247 (1998) [hep-ph/9711395];
R. Rapp, T. Schäfer, E. V. Shuryak and M. Velkovsky, Phys. Rev. Lett. **81**, 53 (1998) [hep-ph/9711396].

[5] K. Rajagopal and F. Wilczek, hep-ph/0011333;
D. K. Hong, hep-ph/0101025;
M. Alford, hep-ph/0003185;
T. Schäfer, Int. J. Mod. Phys. B **15**, 1474 (2001) [nucl-th/9911017].

[6] D. K. Hong, V. A. Miransky, I. A. Shovkovy and L. C. Wijewardhana, Phys. Rev. D **61**, 056001 (2000) [Erratum-ibid. D **62**, 059903 (2000)] [hep-ph/9906478].

[7] T. Schäfer and F. Wilczek, Phys. Rev. D **60**, 114033 (1999) [hep-ph/9906512].

[8] C. D. Roberts and S. M. Schmidt, nucl-th/9903075;
R. D. Pisarski and D. H. Rischke, Phys. Rev. D **61**, 051501 (2000) [nucl-th/9907041];
V. A. Miransky, I. A. Shovkovy and L. C. Wijewardhana, Phys. Lett. B **468**, 270 (1999) [hep-ph/9908212];
I. A. Shovkovy and L. C. Wijewardhana, Phys. Lett. B **470**, 189 (1999) [hep-ph/9910225];
N. Evans, J. Hormuzdiar, S. D. Hsu and M. Schwetz, Nucl. Phys. B **581**, 391 (2000) [hep-ph/9910313];
R. D. Pisarski and D. H. Rischke, Phys. Rev. D **61**, 074017 (2000) [nucl-th/9910056];

M. Matsuzaki, Phys. Rev. D **62**, 017501 (2000) [hep-ph/9910541];
K. Rajagopal and E. Shuster, Phys. Rev. D **62**, 085007 (2000) [hep-ph/0004074].

[9] J. C. Bloch, C. D. Roberts and S. M. Schmidt, Phys. Rev. C **60**, 065208 (1999) [nucl-th/9907086].

[10] J. Berges and K. Rajagopal, Nucl. Phys. B **538**, 215 (1999) [hep-ph/9804233];
K. Langfeld and M. Rho, Nucl. Phys. A **660**, 475 (1999) [hep-ph/9811227];
G. W. Carter and D. Diakonov, Phys. Rev. D **60**, 016004 (1999) [hep-ph/9812445];
A. Chodos, F. Cooper, W. Mao, H. Minakata and A. Singh, Phys. Rev. D **61**, 045011 (2000) [hep-ph/9909296];
H. Mishra and J. C. Parikh, Nucl. Phys. A **679**, 597 (2001) [hep-ph/0003019];
B. Vanderheyden and A. D. Jackson, Phys. Rev. D **62**, 094010 (2000) [hep-ph/0003150];
Y. Kim and M. Rho, nucl-th/0004054;
R. Nebauer and J. Aichelin, hep-ph/0101289.

[11] R. Rapp, T. Schäfer, E. V. Shuryak and M. Velkovsky, Annals Phys. **280**, 35 (2000) [hep-ph/9904353].

[12] D. T. Son, Phys. Rev. D **59**, 094019 (1999) [hep-ph/9812287].

[13] M. Alford, K. Rajagopal and F. Wilczek, Nucl. Phys. B **537**, 443 (1999) [hep-ph/9804403].

[14] M. Alford, J. Berges and K. Rajagopal, Nucl. Phys. B **558**, 219 (1999) [hep-ph/9903502];
T. Schäfer and F. Wilczek, Phys. Rev. D **60**, 074014 (1999) [hep-ph/9903503].

[15] R. D. Pisarski and D. H. Rischke, Phys. Rev. D **60**, 094013 (1999) [nucl-th/9903023].

[16] N. Evans, S. D. Hsu and M. Schwetz, Nucl. Phys. B **551**, 275 (1999) [hep-ph/9808444]; Phys. Lett. B **449**, 281 (1999) [hep-ph/9810514].

[17] T. Schäfer and F. Wilczek, Phys. Lett. B **450**, 325 (1999) [hep-ph/9810509].

[18] R. D. Pisarski and D. H. Rischke, Phys. Rev. Lett. **83**, 37 (1999) [nucl-th/9811104].

[19] V. A. Miransky, "Dynamical symmetry breaking in quantum field theories," *Singapore, Singapore: World Scientific (1993) 533 p*;
T. Kugo, "Basic concepts in dynamical symmetry breaking and bound state problems,"

KUNS-1086 *Lecture delivered at 1991 Nagoya Spring School on Dynamical Symmetry Breaking, Nakatsugawa, Japan, Apr 23-27, 1991.*

[20] T. Kugo and M. G. Mitchard, Phys. Lett. B **282**, 162 (1992).

[21] K. Higashijima, Phys. Rev. D **29**, 1228 (1984);
V. A. Miransky, Nuovo Cim. A **90**, 149 (1985).

[22] K. Aoki, M. Bando, T. Kugo, M. G. Mitchard and H. Nakatani, Prog. Theor. Phys. **84**, 683 (1990).

[23] J. M. Cornwall, R. Jackiw and E. Tomboulis, Phys. Rev. D **10**, 2428 (1974).

[24] Y. Taniguchi and Y. Yoshida, Phys. Rev. D **55**, 2283 (1997) [hep-ph/9512375].

[25] M. Harada and A. Shibata, Phys. Rev. D **59**, 014010 (1999) [hep-ph/9807408].

[26] H. Pagels and S. Stokar, Phys. Rev. D **20**, 2947 (1979).

[27] J. Gasser and H. Leutwyler, Annals Phys. **158**, 142 (1984).

[28] J. Gasser and H. Leutwyler, Phys. Rept. **87**, 77 (1982).

[29] A. Barducci, R. Casalbuoni, S. De Curtis, R. Gatto and G. Pettini, Phys. Rev. D **41**, 1610 (1990).